AD-A132 623 METEOROLOGICAL SENSORS FOR BATTLEFIELD WEATHER SUPPORT 1/1
(U) AIR FORCE GEOPHYSICS LAB HANSCOM AFB MA
F J BROUSAIDES 15 APR 83 AFGL-TR-83-0112

UNCLASSIFIED F/G 4/2 NL

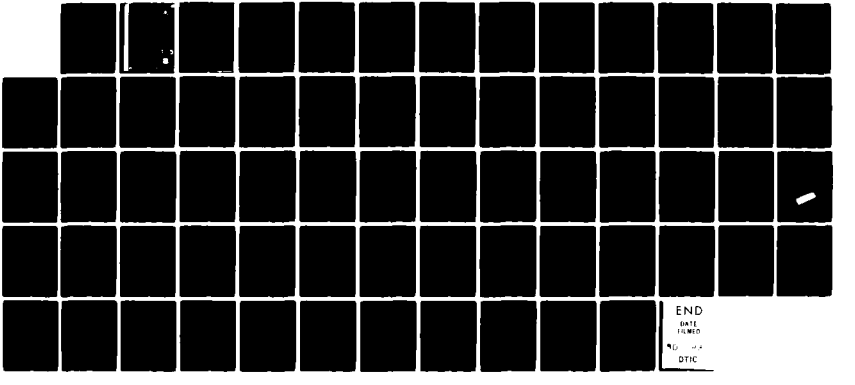

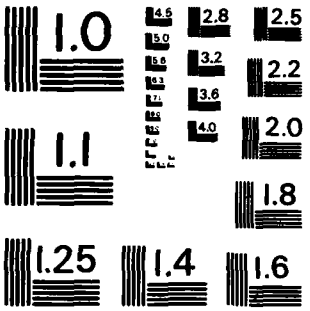

AD-A127 [illegible]

Meteorological Sensors for Battlefield Weather Support

FREDERICK J. BROUSAIDES

15 April 1983

DTIC
S

[redacted]

Unclassified

SECURITY CLASSIFICATION OF THIS PAGE (When Data Entered)

REPORT DOCUMENTATION PAGE		READ INSTRUCTIONS BEFORE COMPLETING FORM
1. REPORT NUMBER AFGL-TR-83-0112	2. GOVT ACCESSION NO.	3. RECIPIENT'S CATALOG NUMBER
4. TITLE (and Subtitle) METEOROLOGICAL SENSORS FOR BATTLEFIELD WEATHER SUPPORT		5. TYPE OF REPORT & PERIOD COVERED Scientific. Final 6. PERFORMING ORG. REPORT NUMBER ERP, No. 836
7. AUTHOR(s) Frederick J. Brousaides		8. CONTRACT OR GRANT NUMBER(s)
9. PERFORMING ORGANIZATION NAME AND ADDRESS Air Force Geophysics Laboratory (LYS) Hanscom AFB Massachusetts 01731		10. PROGRAM ELEMENT, PROJECT, TASK AREA & WORK UNIT NUMBERS 63707F 26880101
11. CONTROLLING OFFICE NAME AND ADDRESS Air Force Geophysics Laboratory (LYS) Hanscom AFB Massachusetts 01731		12. REPORT DATE 15 April 1983 13. NUMBER OF PAGES 65
14. MONITORING AGENCY NAME & ADDRESS(if different from Controlling Office)		15. SECURITY CLASS. (of this report) Unclassified 15a. DECLASSIFICATION DOWNGRADING SCHEDULE

16. DISTRIBUTION STATEMENT (of this Report)

Approved for public release; distribution unlimited.

17. DISTRIBUTION STATEMENT (of the abstract entered in Block 20, if different from Report)

18. SUPPLEMENTARY NOTES

19. KEY WORDS (Continue on reverse side if necessary and identify by block number)

Tactical weather observation
Meteorological sensors
Battlefield weather observation system

20. ABSTRACT (Continue on reverse side if necessary and identify by block number)

The work described in this report is in support of MAC SON 508-78, Pre-Strike Surveillance and Reconnaissance System (PRESSURS), which has identified deficiencies in the Air Force's ability to acquire meteorological observations in uncontrolled and hostile airspace. Primary requirements include temperature, pressure, humidity, winds, cloud field parameters, and visibility. Suitable sensors are identified and evaluated for deployment with various scenarios, that is, remotely-piloted vehicle, dropsonde, and

DD FORM 1 JAN 73 1473 EDITION OF 1 NOV 65 IS OBSOLETE

Unclassified

SECURITY CLASSIFICATION OF THIS PAGE (When Data Entered)

20. Abstract (Contd)

ground implantation. Where deficiencies in the state-of-the-art exist, programs were initiated for the development of new instrumentation, and where necessary, models were constructed for translation of sensor output into useful operational weather information.

Contents

Contents

Illustrations

Tables

Meteorological Sensors for Battlefield Weather Support

1. BACKGROUND

There exists a serious deficiency in our ability to acquire detailed weather and electro-optical measurements in uncontrolled and hostile areas or airspace. These needs were identified in MAC SON 508-78, Pre-Strike Surveillance and Reconnaissance System (PRESSURS), dated 28 December 1978. Target area observations will greatly assist weather forecasters, whose assessments and predictions are often based upon scanty details of general weather conditions. In addition, these observations will provide accurate and timely data that planners require for both target identification and threat assessment. This will permit the maximum utilization of force allocation and optimization of munition loads while reducing the number of weather-diverted and cancelled missions, thus, increasing mission effectiveness.

Increasing use of weather-sensitive Precision Guided Munitions (PGMs), namely, TV, infrared (IR), and, eventually, millimeter-wave systems, also places greater demands upon the quantity and frequency of required weather data. These systems are often critically dependent upon variations in path transmission and contrast transmission. Information on these parameters must come from either direct optical measurements or their inference from related meteorological observables. Also of vital concern to mission planners is the state of any

(Received for publication 8 April 1983)

cloud fields existing in the target area. Low ceilings or significant areal cloud coverage could either seriously impede or curtail air operations.

These needs led to the establishment of the Weather Systems (Advanced Development) Program Element, currently under Program Management Directive, PMD R-S 1029(2)63707F, dated 29 June 82. The PMD title is Battlefield Weather Observation and Forecast System (BWOFS). Specifically identified needs in the target area include clouds (cover, base, and top), path transmission, contrast transmission, wind, temperature, pressure, and humidity from the ground to 10,000 ft. The target area in which observations are required has been arbitrarily defined as being a 50-km square zone up to 200 km beyond the forward edge of the battle area (FEBA). The area from which PRESSURS vehicles could be deployed is at a range from 50 to 150 km behind the FEBA. A list of required weather observables taken from the Combined Employment Concept (CEC) in priority order, along with desired accuracies, is given in Table 1.[1]

The remotely-piloted vehicle (RPV) or autonomously piloted vehicle (APV)* has been identified as the most promising platform for the use or deployment of meteorological sensors. It has the necessary range, endurance, speed, payload, and altitude capability to perform the mission. Most of the emphasis in the BWOFS program is being directed toward solutions utilizing the RPV as the preferred vehicle for tactical weather observation.

Few constraints have been imposed by the PMD for the development of a non-satellite weather observation system. Any technique utilizing RPV, dropsondes, ground implants, rockets, or artillery, and in any combinations, thereof, can be considered. The solution, however, must not commit human observers to hostile areas or airspace. As with any new system, the ultimate cost must be kept as low as possible without compromising accuracy, survivability, or reliability. In keeping with the spirit of providing the user with a broad choice of operational scenarios, several deployment options are being analyzed (by the MITRE Corp.) and, where possible, candidate sensors for these options are identified in this report. Many of these sensors are state-of-the-art and are routinely used at ground installations and in the synoptic weather network; others are under continuing development as part of the BWOFS program. It is anticipated that, after a specific platform(s) has been identified some repackaging and engineering of sensors will be required for their integration into a tactical weather-observation system.

---

*Though APVs refer to those systems (drones) that are preprogrammed and entirely independent. RPVs provide allowance for human control and/or override of trajectory. No distinction between the two acronyms will be made in this report; where RPV is used, APV may also be appropriate.

1. (1982) BWOFS Combined Employment Concept (CEC), Air Weather Service.

Table 1. Weather Observables Requirements

	Accuracy
1. Critical to Tactical Air Force (TAF) operations:	
Cloud cover (lowest deck):	±1/8
Cloud base:	±100 ft (sfc - 1000 ft) ±10% (above 1000 ft)
Slant range visibility (eye):	±20% (0.1 km ≤ vis ≤ 10 km)
Seeability: (that is, maximum slant range at which a PGM or Target Acquisition System (TAS) sensor can perform certain functions, for example, lock-on, acquisition, etc.)	±20% (0.1 km ≤ seeability ≤ 10 km)
2. Enhances TAF operations, but not critical:	
Vertical wind profile:	±10°, ±10 knots
Cloud tops:	±500 ft (tops ≤ 2500 ft) ±20% (above 2500 ft)
3. Useful to TAF operations:	
Surface wind:	±10°, ±5 knots
Surface temperatures:	±1°C
Vertical temperature profile:	±1°C
Surface relative humidity (dewpoint):	±5%
Vertical moisture profile:	±5%
Pressure-derived information: (for example, altimeter setting, pressure altitude, density altitude)	±2%

The intent of this report is to identify sensor candidates, provide general physical descriptions, general performance characteristics, and a rationale for their selection. In those instances where specific commercial instrumentation has been identified, others may also be available that are equally suitable. No attempt has been made to describe the delivery vehicles, that is, RPV, rocket, and artillery, or the operational scenarios in which they would be used; these will be the subject of future reports.

2. HUMIDITY

2.1 Requirements and Options

The choice of humidity sensors for use in a BWOFS system is rather limited and may be deficient in requisite performance. Current sensors, though generally adequate for use in the synoptic radiosonde weather network, often do not have the capability to meet the requirements of the atmospheric physicist or meteorologist. When considering E-O transmission, it should be kept in mind that, the effect of relative humidity can be far greater than the direct impact upon water vapor absorption or continuum absorption. Above 90 percent small variations in relative humidity have an inordinate effect upon aerosol growth characteristics and, hence, transmission. Such information would be valuable in a NOWCAST for estimation of PGM performance. Due to the very wide dynamic range of conditions to which the sensor may be exposed, the development of suitable instrumentation is both challenging and frustrating. A very large variety of techniques for the measurement of humidity may be found in the literature.[2,3] The aforementioned references, though well over ten years old, still represent the state-of-the-art.

Of the major categories of sensors, the electric hygrometers have the most potential for satisfying tactical requirements. In these devices, sorption and desorption of water vapor, by suitably hygroscopic materials, are related to corresponding changes in an electrical characteristic such as resistance. They are of themselves often small, economical, and require relatively unsophisticated circuitry. Current accuracy of electric hygrometers is at best 3 to 6 percent RH, depending upon ambient temperature and the degree of saturation. For forecasting purposes the accuracy is satisfactory. However, if the information is needed for a NOWCAST, in order to characterize the atmosphere for PGM support, it might be inadequate.

Three modes of deployment are contemplated, namely, airborne, dropsonde, and ground implant. Each of these has its own requirements for sensor performance in terms of measurement range and speed of response. The temperature and humidity range requirement is essentially the same for all three modes of deployment. The sensor should perform over a temperature range of about +40 to -25°C and over a range of 10 to 100 percent RH. A ground-implanted sensor need not have a particularly fast response to fluctuations in humidity. A 90 percent response lag of several minutes would be acceptable. For airborne deployment,

---

2. Wexler, A., Ed. (1965) Humidity and Moisture, Volumes I-IV, Reinhold Publishing Corp., N.Y.
3. Wexler, A. (1970) Measurement of humidity in the free atmosphere near the surface of the earth, AMS Monograph II(No. 33):262-282.

however, one must take into consideration both the required vertical/horizontal resolutions required and the speed of the vehicle. It may be assumed for BWOFS requirements that upper-air humidity is homogeneous in the horizontal throughout the target area. Thus, if the sensor is monitoring humidity at constant altitude, requirements upon its speed of response can be relaxed considerably. However, if the sensor is monitoring the environment in a vertical profile mode, either through deployment by RPV or dropsonde, the lag response becomes more critical. Typical dropsonde velocities are from 1000 to 3000 ft/min, depending upon the amount of retardation used and restrictions placed upon the loiter time allowed for the required communications vehicle. These dropsonde velocities are comparable to ascent/descent rates of state-of-the-art RPVs except for some higher performance models.

The CEC does not specify the requisite vertical resolutions for all observed weather parameters. In keeping with current sensor capabilities, this resolution, as an interim goal, will be assumed to be 1000 ft. If the candidate sensor, as in the case of the electric hygrometers, is of the relative-humidity type, then absolute humidity or dewpoint, of course, is a derivable quantity provided that ambient temperature is also available.

One of the BWOFS RPV deployment scenarios specifies the use of an in-situ sensor, currently under development by AFGL (see Section 6.2, The HSS Visibility Meter), used for the estimation of areal cloud cover and ceiling. However, operational constraints prevent the vehicle from descending to an altitude low enough to completely satisfy observational requirements. To overcome this deficiency, an alternative method must be considered for the first 300 to 500 ft above ground level (AGL). One such alternative for the determination of ceiling potential would be its inference from a measurement of the condensation level. This characterization would be possible using state-of-the-art hygristors only if descent rates do not exceed 1000 ft min^{-1} so that the vertical resolution of humidity is kept within the requisite 100 ft for the lowest altitude regime of interest. More information on the vertical resolution as a function of deployment velocity is given in Section 2.3.

2.2 The Carbon Humidity Element

The carbon humidity element has been the principal sensor used in the upper-air U.S. synoptic weather network for over twenty years. In spite of a number of well-documented deficiencies, it is generally satisfactory, and probably will be the sensor of choice in this country for some years to come.[4]

---

4. Brousaides, F.J. (1973) An Assessment of the Carbon Humidity Element in Radiosonde Systems, AFCRL-TR-73-0423, AD 768672.

For special applications, where improved lag response, accuracy, or resolution is required, the need for suitable research-grade hygrometers remains unfilled.

The carbon element is a thin strip of plastic, 2-1/2 in. long, 11/16 in. wide, and coated with a hygroscopic mixture (hydroxyethylcellulose) containing a suspension of finely-divided carbon particles to provide a path for electrical conduction. Changes in relative humidity result in bulk-film volume variations due to the sorption or desorption of water vapor. These changes result in dimensional changes between carbon granules. The overall effect is such that, at high humidities, particle separation is greatest and the resistance is maximized. The long edges of the strip are metalized to provide for an electrical connection to the film. Since conduction in the sensor is due to fixed paths between carbon granules, and is not due to the movement of ionic species in the film, it is not subject to effects of polarization. Whereas, quite a few thin film humidity sensors require the use of ac circuitry to obviate these effects, the carbon element can be utilized in dc circuits.

Typical resistance curves as a function of temperature and relative humidity are shown in Figure 1. Resistance ratio is defined as

$$\frac{\text{resistance at } X\%\ \text{RH } (T^{\circ}C)}{\text{resistance at } 33\%\ \text{RH } (T^{\circ}C)} .$$

Nominal resistance values for the hygristors are 20,000 ohms in the military version (MIL-476) and are somewhat lower in the National Weather Service (NWS) version. Currently, the only manufacturer of these sensors is the VIZ Manufacturing Co., Philadelphia, Pa. The hygristor is commercially available in hermetically-sealed cans and can be supplied precalibrated.

The carbon-element humidity lag response as a function of temperature is significant and, at the end of its useful temperature range of operation (that is, $-40^{\circ}C$), can be as long as 5 to 10 min. Table 2 was prepared from data published by Marchgraber and Grote[5] which, in spite of some manufacturing changes, may still be considered representative of current performance.

Utilization of the carbon element requires that it be carefully shielded to obviate the effects of insolation. The black film is an efficient absorber of

5. Marchgarber, R.M., and Grote, H.H. (1965) The dynamic behavior of the carbon element, MIL-476, Humidity and Moisture, A. Wexler, Ed., Reinhold Publishing Corp., N.Y., pp. 331-345.

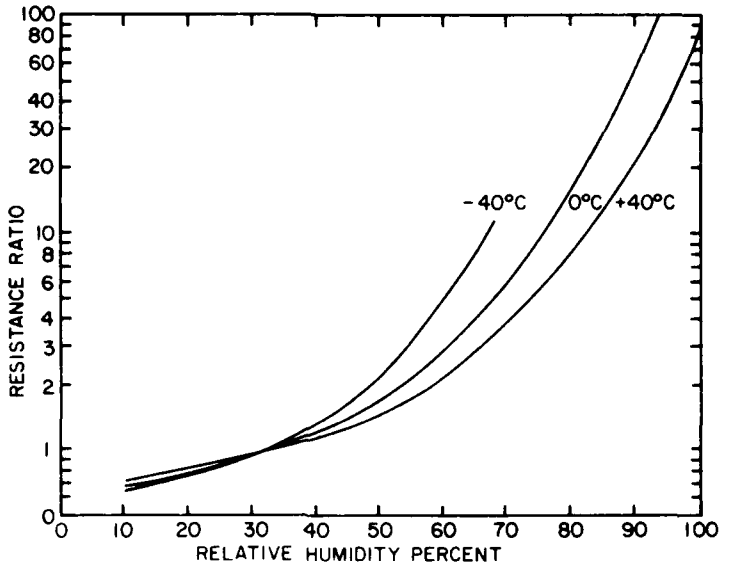

Figure 1. Carbon Hygristor Response – Humidity Isotherms

Table 2. Carbon Humidity Element Response

Direction	Temperature	50% Response	90% Response
RH↑	+25°C	0.3 sec	1.0 sec
RH↓		0.2 sec	2.9 sec
RH↑	-5°C	0.85 sec	20 sec
RH↓		1.60 sec	48 sec
RH↑	-20°C	2.1 sec	78 sec
RH↓		4.6 sec	120 sec

RH↑ - increasing relative humidity
RH↓ - decreasing relative humidity

radiation that results in a rise of sensor temperature with attendant temperature-induced humidity errors.[6] Before this problem was recognized, the error in U.S. radiosonde upper-air humidity measurements was as high as 50 percent. This requirement for shielding will impose some difficulty in its deployment by

6. Morrissey, J.F., and Brousaides, F.J. (1970) Temperature induced errors in the ML-476 humidity data, J. Appl. Meteorol. 9:805-808.

dropsonde. In this mode, size, weight, and overall configuration are critical design details. General performance characteristics for the carbon hygristor may be found in an article by Stine.[7]

Temperature-induced humidity errors, in general, result from the fact that changes in air temperature significantly alter the saturation vapor pressure. Thus, a change in the air temperature in contact with the sensor results in a concomitant change of its relative humidity. If the sensor is of the relative humidity type, it will respond to this "apparent" change of condition. Considering the inherent accuracy of the hygristor, if the error is sufficiently large to warrant its correction, this can be accomplished as long as the hygristor temperature is known. The assumption is made that the air temperature in immediate contact with the hygristor, and to which the sensor responds, is at the same temperature as the hygristor. A small bead thermistor can readily be embedded into the hygristor substrate to monitor this condition. The corrected humidity can be calculated from the following relationship:

$$RH_c = \frac{e_{swh}}{e_{swa}} RH_m \quad , \tag{1}$$

where

RH_c is actual humidity,

RH_m is measured humidity,

e_{swa} is saturation vapor pressure at free air temperature, and

e_{swh} is saturation vapor pressure at hygristor temperature.

Saturation vapor pressure may be calculated by:

$$e_s = 6.1078 \exp\left[\frac{17.269T}{T+237.3}\right] ,$$

where T is in degrees Celsius and e_s is saturation pressure over water expressed in millibars.

It should be noted that an induced humidity error will always result from an imbalance between sensor and air temperature, regardless of the mechanism for the imbalance. Thus, if the hygristor is exposed, as it usually is, during an upper-air sounding, to either ramp or step function changes in air temperature,

7. Stine, J. L. (1965) Carbon humidity elements—Manufacture, performance and theory, Humidity and Moisture, A. Wexler, Ed., Reinhold Publishing, N. Y., pp. 316-330.

there will be induced humidity errors due to sensor thermal lag. These errors could be significant if the sensor is deployed on a rapidly-descending dropsonde. To assess the magnitude of such errors, consider the response of a sensor to an atmosphere whose temperature is varying linearly with height on a dropsonde descending at a constant velocity. Thermal lag can be related to the function,[8]

$$T - (T_1 - \beta t) = (To - T_1)\, e^{-t/\lambda} - \beta\lambda(1 - e^{-t/\lambda}) \quad , \tag{2}$$

where T_1 and To are initial sensor and air temperature, respectively, λ is the sensor response time (pressure dependent), and β is the temperature rate of change to which the sensor is exposed. This equation may be rewritten to yield,

$$\Delta T \quad \Delta T_o(e^{-t/\lambda}) - \beta\lambda\,(1 - e^{t/\lambda}) \quad , \tag{3}$$

where ΔT is $(T_{sensor} - T_{air})$ and ΔT_o is the initial difference. After several time constants, at a constant lapse rate, this equation reduces to the steady-state condition, $\Delta T = -\beta\lambda$. If we assume temperature lapse rate of $3^{o}C/1000$ ft, a dropsonde descent velocity of 3000 ft min^{-1}, and a hygristor thermal lag, λ, of 15 sec, then

$$\Delta T \quad -(9^{o}\,min^{-1})(0.25\,min) \quad -2.3^{o}C \quad . \tag{4}$$

An error of $-2.3^{o}C$ implies an absolute humidity error of approximately 10 percent RH, depending upon the air temperature. Thus, it is evident that carbon hygristor deployment by dropsonde, at stated descent rate, would require correction for thermal lag.

2.3 The Vaisala Humicap

The Vaisala Humicap sensor is a polymeric thin film sensor utilizing capacitive readout. The sensor was designed for, and is marketed by, the Finnish radiosonde manufacturer, Vaisala Inc.

The configuration of the Humicap is shown in Figure 2.[9] According to product literature, lower electrodes (B) are etched into a metalized glass plate (A), coated with a thin film of hygroscopic organic polymer (C), upon which a porous metal upper electrode (D) is deposited. In current design, three pairs of interdigitated electrodes are deposited, instead of the single pair shown in the figure. Overall

---

8. (1956) Handbook of Meteorological Instruments, Part I. Her Majesty's Stationery Office, London.

9. (1975) New Thin Film Sensor, Vaisala Ref. No. B235, Vaisala, Inc.

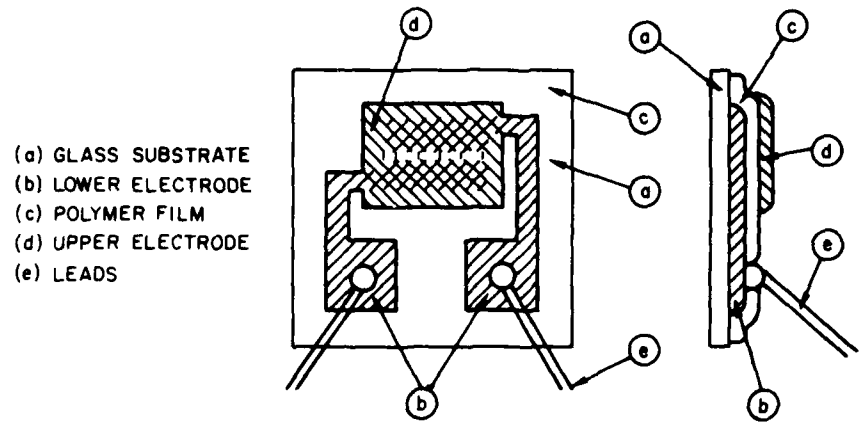

Figure 2. Vaisala Humicap Configuration

dimensions of the sensor are 6 × 4 × 0.2 mm. The sensor was developed for use in a capacitance mode since other sensors on the Vaisala radiosonde are also of this type.

Humicap performance and characteristics, as provided by Vaisala Inc., are given in Table 3. Though these data are for an industrial sensor, they should be essentially the same as for the radiosonde version. Humicap speed-of-response as a function of temperature is given in Figure 3, and appears to be fairly fast considering that water vapor must first diffuse across a porous electrode. Humidity lag tests and calibrations of the radiosonde have been conducted independently by another U.S. agency.[10]

Findings on a limited number of sensors include the following:

(a) The time required at +25°C for the sensors to attain 63 percent (t_{63}) and 90 percent (t_{90}) of the final humidity value for a step function from 40 to 90 percent RH was 0.3 and 0.7 sec, respectively. In the reverse direction, the lags were 0.3 to 0.7 sec, respectively,

(b) The time required at -30°C for the sensors to attain t_{63} and t_{90} of the final humidity value for a step function from 40 to 70 percent RH was 7.1 and 17 sec, respectively. In the reverse humidity direction, the lags were 8.3 and 20 sec, respectively,

(c) Calibrations indicate a systematic error of 4 to 5 percent RH, and

(d) Average hysteresis shown by the Humicap for calibrations at 25, -2.5, and -30°C were, approximately, 4, 2, and 1 percent RH, respectively, for first

10. Hoehne, W., National Weather Service (1982) Private communication.

Table 3. Humicap 6061 HM Characteristics

Sensitive element:	Thin film capacitor
Humidity range:	0...100% RH
Response time:	About 1 sec to 90% of total humidity change at +20°C
Hysteresis:	Better than ±2% for humidity excursion 0...100...0% RH Better than ±1% for humidity excursion 0...80...0% RH
Linearity:	±1% RH in humidity range 0...80% RH, in humidity range 0...100% RH linearity depends on drift
Accuracy:	±2% RH in humidity range 0...80% RH at +20°C ±3% RH in humidity range 80...100% RH at +20°C, provided that the probe is long-term calibrated and kept continuously in humidity above 80% RH
Temperature coefficient:	About 0.05% RH/1°C

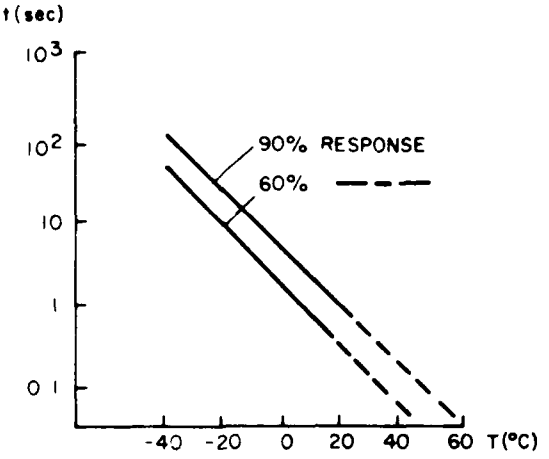

Figure 3. Humicap Speed of Response

calibrations. For subsequent calibrations at the same temperature the hysteresis diminished.

The Humicap, as deployed in the Vaisala sonde, is unshielded; the sensor is projected a few centimeters from the sonde package on a thin, narrow, rigid holder. This manner of deployment would lead one to assume its independence from insolation effects. Though the Humicap probably is not subject to this source of error to the same extent as the carbon element, it is difficult to believe that it is not an issue. Whether or not this is a problem could be readily determined in a duel flight comparison of a Vaisala sonde and an NWS sonde. Alternatively, the same end could be readily served by a few, relatively simple laboratory tests. In any event, this author will assume, until it has been demonstrated otherwise, that some ducting or shielding arrangement is required for its deployment.

One method of shielding that can be given consideration is with the use of porous sintered metal shells. These shells are pervious to the environment and with suitable ventilation, should exchange air rapidly enough to satisfy response requirements. When deployed by RPV or dropsonde, forced ventilation resulting from the motion of the vehicle may be utilized. When deployed as a ground implant, surface winds in excess of 1 to 2 knots should provide sufficient aspiration. Any shielding has the potential for perturbing the temperature of the ambient air and could, thus, induce a humidity measurement error. To permit a correction to be made for this induced humidity error, the air temperature within the humidity cavity must also be monitored; a small bead thermistor will adequately serve this function. The time ambient relative-humidity can be recovered through the use of Eq. (1), where e_{swh} now becomes e_{swc}, the value for saturation at cavity air temperature.

In the utilization of the Humicap in the dropsonde mode, temperature-induced humidity errors due to thermal lag cannot presently be estimated. The error from this source undoubtedly is less than that found with the carbon hygristor due to the Humicap's smaller heat capacity and increased surface area to mass ratio. Figure 4 shows estimates of the spatial resolution anticipated with Humicap use at various deployment velocities and as a function of ambient air temperature.

2.4 Conclusions

Currently available radiosonde-type hygristors are adequate for the characterization of relative humidity when deployed by dropsondes or used in ground implants. This assumes that inherent sensor accuracies are satisfactory and that high dropsonde velocities are not required.

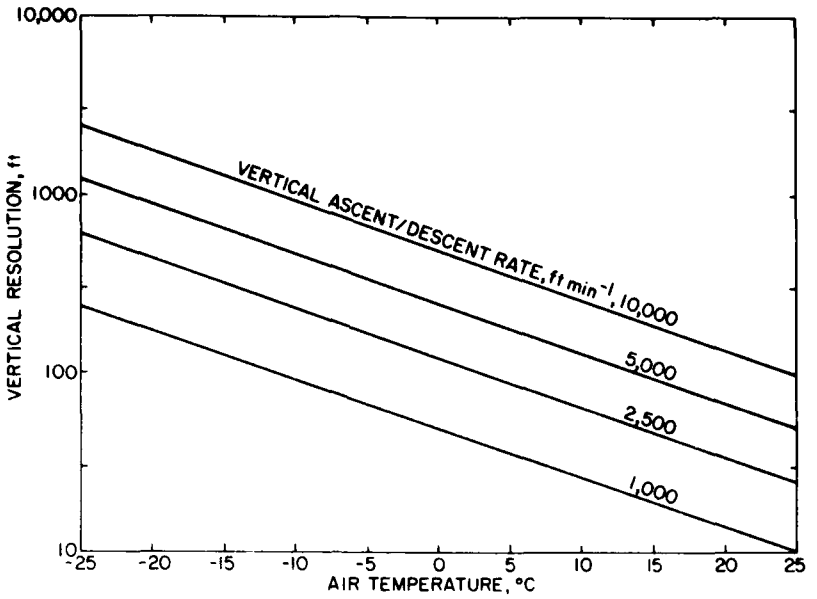

Figure 4. Vertical Resolution of Humidity With the Humicap as a Function of Deployment Velocity and Air Temperature

Deployment of electric hygrometers aboard a high-performance RPV poses a number of special problems. The spatial resolution will, of course, be great due to sensor time-constant considerations. In addition, however, problems associated with aerodynamic heating also have to be addressed. It cannot be overstressed that when utilizing sensors that respond to relative humidity, one must not only be concerned with the ambient air temperature, but also the temperature of the air sensed by the hygrometer. Thus, if an "air-scoop" or probe is used to duct the air sample to the sensor, both temperatures must be measured to permit the calculation of relative humidity.

If greater accuracies and spatial resolutions are desired than are possible using expendable "contact" or "immersion" type sensors, then more sophisticated indirect techniques must be resorted to. One technique that is under consideration is an infrared (IR) spectrometric method, the prototype development for which was supported by AFGL's Cloud Physics Branch.[11] In this method, absolute humidity is measured by the differential IR absorption of a reference wavelength at 2.45 μm and the water vapor band at 2.67 μm. Projected accuracy is 2 percent over a dynamic range of 0.01 to 50 g m^{-3} with a sampling rate of about 25 hz.

11. Nelson, L. D. (1982) Theory, Electro-optical Design, Testing, and Calibration of a Prototype Atmospheric Supersaturation, Humidity, and Temperature Sensor, AFGL-TR-82-0283, AD A121713.

3. FREE AIR TEMPERATURE

3.1 Requirements

Of the meteorological observations required for BWOFS, the measurement of free air temperature presents the least problem. The current state-of-the-art can provide for greater accuracy and faster time response than is needed. Therefore, the use of platinum resistance thermometers having millidegree Celsius accuracy, or fine resistance wires that have millisecond time constants are not warranted here. Realistic goals for a BWOFS temperature sensor are 0.2 to 0.3°C accuracy and a time constant of several tenths of a second for RPV deployment (possibly longer for dropsonde deployment). The most useful class of thermometers for our specific purpose is the thermistor. General properties and characteristics of this type of sensor are provided in this report.

3.2 The Thermistor

Thermistor is a contraction for "thermally sensitive resistor." These are semiconductor materials made from various metal oxides, such as manganese, cobalt, and nickel, which are molded, compressed, and fired at high temperatures to produce a ceramic-like substance with stable temperature/resistance characteristics. Wire conduction leads are usually incorporated into the material prior to the firing process. They are available from a large number of manufacturers and may be supplied in a wide range of shapes, for example, rods, beads, discs, washers, and films, as well as in a variety of sizes.

Thermistor resistance is purely ohmic and, in contrast to most other materials, has negative coefficients of resistance. That is, the resistance increases with decreasing temperature. The range of resistances available for a given temperature range is large and, if necessary, can be tailored to fit specific requirements.

The resistance, R, of a thermistor can be shown to obey the general relationship,

$$R = b\, e^{\frac{a}{T}} , \tag{5}$$

where a and b are constants and T is the absolute temperature. Two other useful equations are:

$$\frac{R_o(T_1)}{R_o(T_2)} = e^{\beta\left(\frac{1}{T_1} - \frac{1}{T_2}\right)}, \tag{6}$$

where β is a constant that depends upon the composition of the thermistor, and

$$\alpha_T = \frac{1}{R_T} \frac{dR_T}{dT} \text{ ohms/ohm/}^{\circ}\text{C} \cong -\frac{\beta}{T^2} \quad , \tag{7}$$

where α_T of a thermistor is a measure of sensitivity to temperature variation at a given resistance.

If the environmental temperature range of interest to BWOFS is approximately +40 to -40°C, the degree of resolution required in the monitoring of equivalent resistance may be found in an examination of the characteristics of available commercial thermistors. Assuming that the nominal resistance of the sensor (that is, resistance at +25°C) is in the range of 3,000 to 30,000 ohms, then corresponding resistances for the given range of temperature would be about 1.5 to 100 kohms, and 15 kohms to 1 Mohms, respectively. Alpha values for a representative thermistor from one manufacturer were -3.9 and -8.6 percent/°C for temperatures of +40 and -40°C, respectively.

In the early 1970s, the performance of various temperature-sensor options that were considered viable by the NWS for their projected upgraded upper-air sounding system, Next Generation Upper Air System (NEXAIR), were evaluated. These options are shown in Table 4 and are still typical of the state-of-the-art.[12] The table indicates the extent of important error sources, namely, calibration, solar, and IR errors. Calibration errors are considered biases that can be accounted for in a base-line correction. Solar errors are always positive and are, of course, not present at night. Infrared errors may be present day or night and are due to temperature differences between the sensor and the surrounding environment. Figure 5, from the NEXAIR report, is a graphic representation of these error sources for the standard rod thermistor. If we were concerned with the accurate monitoring of temperature from the ground to 100,000 ft, radiation errors would have to be taken into account. Since altitudes below 10,000 are of prime concern in BWOFS, such concern is not warranted. The thermistor, however, should be coated with either aluminum, gold, or lead-carbonate paint to minimize these errors and be provided with a good calibration.

For BWOFS application, the standard rod thermistor, Rod No. 1, is somewhat slower than desired and, as with Rods Nos. 2 and 3, is not as robust as some of the available bead thermistors. The resistance wire thermometer, which is used in special Japanese "reference radiosondes," is very fast, but has

12. (1971) Final Report—NEXAIR Design Analysis, SDO Report 9, NOAA, National Weather Service.

Table 4. NEXAIR Candidate Temperature Sensors

Type	Rod No. 1[1]	Rod No. 2	Thermistor Rod No. 3	Wafer	Bead	Resistive Wire NiFe
Size (in.)	0.05 D 2.00 L	0.025 D 1.00 L	0.025 D 1.00 L	0.025 Thick 0.080 Wide	0.014 D	0.0008 D[2] 39.4 L
Coating	$PbCO_3$	$PbCO_3$	Al	Au[3]	Al	None
Base-line Check Required	Yes	Yes	Yes	No	No	Unknown
Time Const (sec)[4]						
0 km	4.5	1.5	1.5	1.0	0.1	0.01
3 km	5.0	1.7	1.7	1.1	0.1	0.01
7 km	6.5	2.3	2.3	1.4	0.2	0.01
24 km	18.0	6.8	6.8	3.5	0.3	0.03
30 km	29.0	10.0	10.0	5.0	0.4	0.05
rmse (°C)[4]						
3 km						
Calib	0.20	0.20	0.20	0.07	0.03	0.03
IR	0.03	0.00	0.00	0.00	0.00	0.00
Solar	0.30	0.20	0.40	0.60	0.04	0.00
9 km						
Calib	0.20	0.20	0.20	0.07	0.03	0.03
IR	0.10	0.00	0.00	0.03	0.00	0.00
Solar	0.40	0.30	0.50	0.80	0.05	0.00
24 km						
Calib	0.20	0.20	0.20	0.13	0.03	0.03
IR	0.40	0.30	0.03	0.07	0.10	0.00
Solar	0.90	0.70	1.10	2.30	0.00	0.10
30 km						
Calib	0.20	0.20	0.20	0.13	0.03	0.03
IR	0.80	0.60	0.07	0.10	0.00	0.00
Solar	1.30	0.90	1.50	3.60	0.14	0.20

1. Present NWS Radiosonde Sensor
2. Size of assembled unit: 2.75 in. × 4-1/4 in.
3. Ship stock leads gold-plated; wafer not coated
4. Assumes a 5 m/sec. ascent in the standard atmosphere

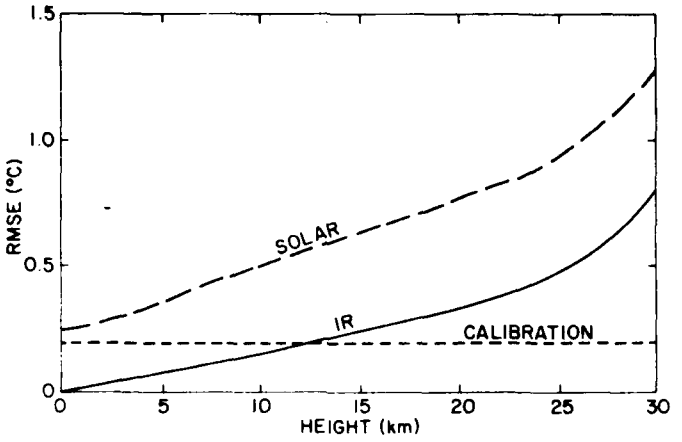

Figure 5. Radiation-induced Temperature Errors for the Rod Thermistor

the disadvantage of being quite fragile and does not exhibit the large variation in resistance with temperature change that is found with thermistors.

A 0.014 bead, though fragile in handling, can very adequately withstand the rigors of rocket or dropsonde deployment. Also, if deployed by dropsonde at a velocity of 3000 ft/min it will provide for spatial resolution of about 150 ft.

Currently-available thermistors are very stable and need not be recalibrated prior to use. For a nominal cost, of about one dollar per calibration point, many manufacturers will supply thermistor calibrations. Depending upon the range of interest and the accuracy requirements, one to three calibration points are usually required. For an upper-air sounding from the ground to 30 km, three calibration points might be necessary. For a more restricted temperature range, such as for BWOFS, one or two points should be adequate.

When using small bead thermistors to sense the atmosphere, the electrical conduction leads become important contributors to thermal lag, particularly at high altitudes, where convective heat-transfer coefficients become smaller. Short leads attached to relatively massive mounts can induce significant lags, which normally can be minimized by utilizing thermistors have relatively long leads. Again, since we are concerned with monitoring the lower atmosphere, the perturbations that would be associated with shorter leads is not significant. This latter fact is of practical importance since small thermistors customarily are supplied with short leads (typically 5/16 to 3/8 in.).

Three useful thermistor mounting arrangements are shown in Figure 6. In Figure 6(a) thermistor leads are soldered to electrical conductors plated on thin

phenolic or fiberglass board. An arrangement similar to this has been used on Super Loki meteorological rocketsondes. Figure 6(b) shows a nonconductive rod with plated leads. Figure 6(c) is a mount used in gas chromatographic instruments and could be acceptable for use on dropsondes or RPVs.

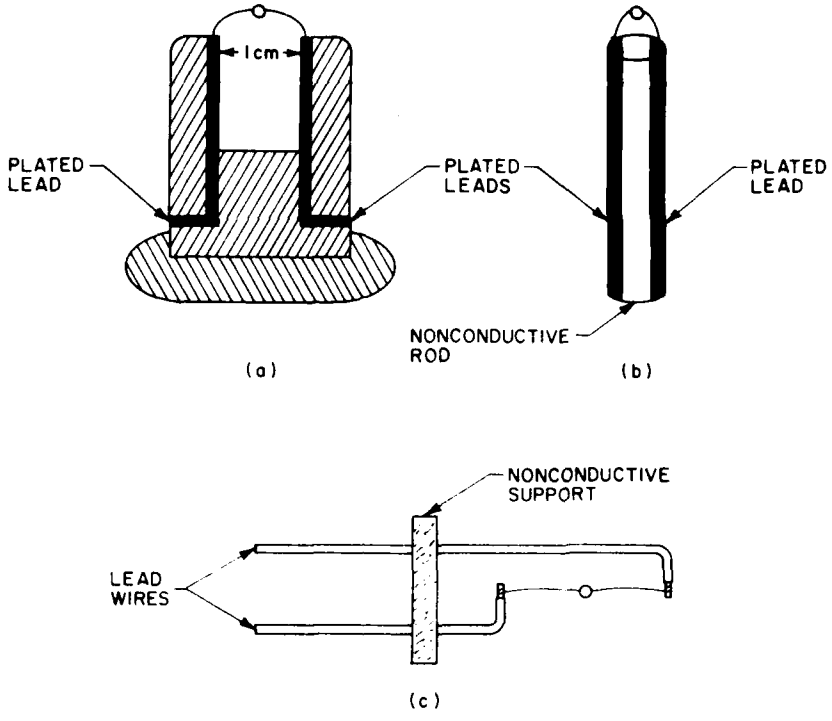

Figure 6. Bead Thermistor Mounting Configurations

3.3 Dynamic Heating Effects and Sensor Location

When the temperature of a fluid is in motion relative to a probe, the observed measurement will depart from this value depending upon the extent to which kinetic energy is dissipated upon the probe. The temperature departure (always positive) will be at a maximum if air is brought completely to rest, adiabatically, with complete conversion of kinetic energy into thermal energy. The maximum temperature rise, dynamic temperature, is related to total temperature (commonly referred to as stagnation temperature) by the following relation:

$$\frac{T_o}{T_\infty} = 1 + \frac{\gamma - 1}{2} M^2 \quad , \tag{8}$$

where

T_o = total temperature,

T_∞ = ambient (static) temperature,

γ = Cp/Cv ≅ 1.4 for air, and

M = Mach number.

It can be seen from Eq. (8) that a correction for dynamic temperature rise becomes an important concern for BWOFS application only at sensor velocities in excess of several thousand feet per minute. For example, at an indicated airspeed of 4000 ft/min (M 0.06), the expected temperature rise will be about 0.25°C. Thus, for any reasonable and expected dropsonde velocity, dynamic heating can be ignored. Where air temperature would be monitored aboard an RPV, the maximum climb rate for any vehicle currently under consideration for this program, is 10,000 ft/min. At this velocity, the temperature rise could be about 1.5°C. The actual temperature rise experienced by a probe in the real-world will be determined by its design and location on the vehicle; this would be established in wind tunnel testing.

4. ATMOSPHERIC PRESSURE

4.1 Requirements

There are three potential platforms for BWOFS pressure sensor deployment, namely, dropsonde, RPV, and ground implant. Each of these modes encompasses a different pressure range that might require different instrument accuracies and/or performance characteristics. For vertical profile monitoring from a dropsonde, whether delivered by rocket/artillery or RPV, the range of interest is from 0 to 10,000 ft AGL. A sensor range of approximately 1100 to 600 mb (0 to 14,000 ft MSL) would satisfy the requirements for most locations in NATO countries. Though the measurement range for a ground implant is more limited than for upper-air profiling, the size, weight, and power requirements should be similar. It is quite likely that, the same pressure sensor with some range tailoring could be used for both of the aforementioned purposes. The sensor aboard an RPV, however, in addition to monitoring barometric pressure, might have to double as a pressure altimeter for control and guidance purposes.

If a line-of-sight requirement exists for communication, either because of data store-and-forward requirements or for navigation update purposes, the pressure range might be extended to 150 mb (45,000 ft). Specifications for any pressure sensor should ensure for adequate protection against overpressure, irrespective of the specific pressure range being monitored by that instrument.

With the possible exception of manometric techniques, which are normally useful only at fixed surface locations, the most common barometers are of the aneroid type, that is, without liquid. Aneroid barometers utilize elastic elements in the form of diaphragms, bellows, tubes, etc. These transducers may have direct mechanical outputs with linkaged dials or pointers, or have passive electrical outputs such as capacitance pickups, linear differential transformers, or strain gages. A major advantage of electrical vs strictly mechanical readout is that linkage friction and wiper arm friction across commutator plates having plated conductor contacts are eliminated. Also, electrical pickup permits the availability of continuous readout or infinite resolution.

Over the years, literally millions of aneroid capsules have been used in standard radiosondes in the synoptic weather network. These barometers have linked wiper arms and are somewhat larger than desired for use in a dropsonde. Since mechanical linkages probably would not survive high G forces, they also are not candidates for use in a ground-implant system. Because of the extensive use and available history of these aneroid pressure cells, their performance is a useful reference point for comparison with alternative sensors. The pressure error estimate, given by the Range Commanders Council/Meteorology Group, varies linearly with altitude from 0.1 percent at the surface to 1 percent at 30 km.[13] In an analysis of 50 dual rawinsonde releases (both instruments on the same flight train), the NWS determined the functional precision* of the aneroid capsule to be ±1.9 mb for sensors compared at the same time.[14] Since upper-air synoptic pressure data is obtained only in a decreasing pressure regime, this obviates some of the problems associated with hysteresis. Also, as a part of prelaunch calibration procedures, pressure cells are adjusted to match the station surface pressure; this further reduces various error sources.

Candidate sensors for different BWOFS deployment options are described in the following section. Specific sensors ultimately selected will depend upon

---

*Functional precision was defined as the rms of the difference between readings from two or more identical sensors operating in the same environment.

13. (1981) Meteorological Data Error Estimates, Meteorological Group, Range Commanders Council, Document 110-81.

14. Hoehne, W. E. (1980) Precision of National Weather Service Upper Air Measurements, NOAA Tech. Memo. NWS T&ED-16, Sterling, Va.

additional performance data as it becomes available and upon deployment constraints as they become defined.

4.2 Dropsonde/Ground-Implant Sensors

4.2.1 ANEROID CAPACITANCE SENSORS

The displacement of a diaphragm in an aneroid capsule can be used to vary the separation between plates of a capacitor. Through calibration, capacitance can be related to a measure of pressure. Though a wide range of these sensors are commercially available for a variety of applications, not many are suited for upper-air atmospheric monitoring. In addition, for those sensors having apparently acceptable characteristics, there is a dearth of published test data that would enable one to make an informed assessment of their potential to BWOFS.

Atmospheric Instrumentation Research, Inc., (AIR), currently markets a miniature aneroid cell with capacitance readout. The cell is approximately 1 in. square and 1/8 in. thick; a larger cell (2 in. × 1/4 in.) is also available. AIR product literature indicates that a bead thermistor mounted on the pressure cell is used for temperature compensation. The stated precision of this smaller sensor system is 3 mb. As with other aneroid cells having electrical output, measurement accuracy can be increased if supply voltage and sensor/circuitry temperature are monitored and accounted for in the transfer equation.

It is the author's understanding that a current Air Force procurement has been initiated that will specify the 2 in. × 1/4 in. AIR capacitance pressure cell as the approved sensor for approximately 500 Omega dropsondes.

Vaisala, Inc., of Finland utilizes capacitance pressure cells in their RS-80 and WS-80 sondes. Product literature indicates a measurement range of 1060 to 3 mb with a resolution of 0.1 mb and a calibration repeatability of ±0.5 mb. The pressure cell has a diameter of 30 mm and weighs 5 g.

4.2.2 ANEROID PIEZORESISTANCE PRESSURE SENSOR

In piezoresistive pickup of aneroid cells, strain-sensitive resistors can be embedded in the surface of the diaphragm to sense its position. In a development for the Navy, Honeywell, Inc., has designed a lightweight meteorological sonde (Mini-Refraction Sonde) for the measurement of atmospheric index of refraction.[15] This sonde utilizes a miniature (7.5 g) solid-state device from their Microswitch Division as the pressure transducer. To compensate for temperature sensitivity, the strain-sensitive resistors are used in a bridge circuit. For additional compensation, a thermistor is used to monitor electronic circuitry temperature, and an

15. Motchenbacher, C. D. (1977) Mini-Refraction Sonde Laboratory Tests, NADC-76128-30-A.

18 constant algorithm is used to calculate ambient pressure. Each pressure cell is individually calibrated in terms of temperature, pressure, and supply voltage. Honeywell claims an rms pressure accuracy of ±1 mb.

4.3 RPV In-Flight Pressure Sensor

As previously mentioned, an autonomous pressure sensor is not necessarily required aboard an APV/RPV. If a pressure altimeter is used in the guidance system, it would adequately serve as a meteorological sensor. Such a unit would not need to be expendable and could be expected to have improved accuracy over sensors used in a dropsonde or ground implant. The characteristics of two potential instruments, both of which are manufactured by Rosemount, Inc., are given in Table 5.

Table 5. Rosemount Pressure/Altitude Transducers

1. Rosemount Model 12011 Pressure Transducer

   This unit was designed for ground and airborne barometric pressure measurement.[16] Some of the pertinent specifications are as follows:

Temperature range:	-55 to +71°C
Input power:	±15 or +28 Vdc
Output voltage:	0 to +5 Vdc and 0 to +10 Vdc
Weight:	±15 Vdc option 12 oz ±28 Vdc option 15 oz
Response time (63%):	1.5 ms maximum
Operating accuracy:	Better than ±0.3% full scale pressure. Operating accuracy includes static accuracy, calibration tolerances, and the effect of temperature variation.

2. Rosemount Model 1231B Altitude Transducer

   This unit was designed to provide barometric altitude information aboard aircraft operating in the range of -1000 to 50,000 ft. As an option, this model can be provided with an output for altitude rate of climb or descent. Other pertinent information are given here.[17]

Input power:	+15 and -15 Vdc
Output voltage:	0.1 and 0.2 mv/ft
Temperature range:	-55 to +71°C
Time constant (63%):	<50 ms at sea level
Operating accuracy:	±0.4% of reading plus 20 ft (or ±5 mv, whichever is greater). Accuracy includes, resolution, hysteresis, non-linearity, and calibration tolerances
Temperature error band:	±1.5% of reading plus 65 ft (or ±12 mv, whichever is greater).

16. Rosemount Product Data Sheet 2339, Rosemount Inc.
17. Rosemount Product Data Sheet 2064, Rosemount Inc.

5. WINDS

5.1 Upper Air Winds

The observation of winds in support of Air Force operations in the target area is currently limited to that obtained from pilot reports. These observations are limited and, in general, are unsatisfactory. The PRESSURS Statement of Need (SON-508-78) calls for winds in the target area from the ground to 10,000 ft. Further definition of requirements developed in the revised CEC for the BWOFS program have relegated upper-air winds to a priority-three category of importance.

Because of the lower priority assigned to upper air winds, and some problems associated with their observation in a tactical weather system, the higher priority BWOFS requirements have been given precedence. It should be noted, however, that if a wind measurement is desired aboard an RPV/APV, a variety of techniques are available. These methods presume the knowledge of airspeed, heading, and groundspeed (or position and time from NAVAIDs). The technique is of limited value, since one obtains wind only at flight altitude and in some scenarios the vehicle must be constrained to specific flight patterns; it is described, however, for purposes of completeness in treatment. Several computer programs for the computation of winds from an instrumented Aquila-type RPV are described in a report by Cogan.[18]

The accuracy of wind velocity measurements (or even the ability to make them) will be a function of subsystem NAVAID capability, as well as the velocity of the vehicle; an analysis of projected capability must await the specification of the PRESSURS navigational system. At present, navigation and communication systems for BWOFS alternatives are still under evaluation. It would appear appropriate to initiate a detailed analysis of measurement potential and additional sensor requirements after such a system has been selected. It may be reasonably anticipated that, whatever navigation system is required for successful deployment of a BWOFS such as, the Modular Integrated Communications and Navigation System (MICNS), the Global Positioning System (GPS), or an Inertial Guidance System (INS), it will have some capability to provide inputs for the computation of winds. Certainly, groundspeed and barometric pressure will be available information. If airspeed cannot be determined from flight-control instrumentation, various commercial sensors are available. These sensors often depend upon pressure measurements taken with Pitot tubes. Pitot tubes are constructed such that measurements of static pressure (ambient barometric pressure) and total pressure (impact pressure plus static pressure) can be made. The difference

---

18. Cogan, J.L. (1981) Techniques for the Computation of Winds Using RPV Flight Data, White Sands Missile Range, ASL.

between impact pressure and static pressure is a measure of windspeed. Thus, indicated airspeed (IAS) may be written,

$$IAS = \left[\frac{P_{Total} - P_{Static}}{f(P_{Total} - P_{Static})} \right]^{1/2} \quad (9)$$

The denominator in Eq. (9) is a function relating differential pressure to fluid velocity over a specific range of velocities. Since IAS is equal to the desired quantity, true airspeed, only at standard sea level conditions, corrections for air density and temperature are also required.

The Rosemount Model 542K1 Altitude/Airspeed Transducer is typical of commercially-available sensors and has characteristics suitable with the anticipated operational envelope for a BWOFS.[19] Pertinent characteristics are given in Table 6.

Table 6. Rosemount Model 542K1 Altitude/Airspeed Transducer

Operating range:	-1000 to 40,000 ft for indicated airspeeds from 125 to 550 knots
Operating accuracy:	
Height:	±40 ft + 0.7% of reading
IAS:	±3.5 knots or 1.0% of reading
Impact pressure (qc):	±0.5% full scale +1.0% of reading
Impact voltage:	+28 Vdc
Time constant:	20 msec (63%)
Operating temperature range:	45 to +160°F
Weight:	2 lb

It should be noted that, barometric pressure or pressure altitude will also be available from airspeed sensors utilizing the Pitot tube principle.

Vertical wind profiling through the tracking radiosonde/dropsonde packages using NAVAID signals, such as Loran-C or Omega, is a mature technology. The literature is replete with information on theory techniques, and field-test results.[20-23]

Because of the large number of references cited above, they will not be listed here. See References, page 61.

The rms Omega wind vector error estimated by Weiss and Morrissey[22] for a 1-min averaging interval was found to be 3.2 m sec^{-1}. Assuming a reasonably rapid dropsonde descent of 2000 to 2500 ft min^{-1}, which is necessary to minimize the sonde-RPV separation distance and also keep the package close to the target area, this distance will also be the spatial resolution of the vertical wind profile. The use of Loran-C could improve profiling accuracy. However, if NAVAIDs are to be considered for upper-air wind finding in a tactical NATO environment, the relative susceptability of various NAVAID frequencies to electronic countermeasures (ECM) will also have to be taken into account. Loran-C coverage in Europe is said to be poor due to an RFI source located in Prague, Czechoslovakia. In the aforementioned report, the use of Loran-D NAVAIDs is also said to be of dubious value over the use of Omega because of the rapid degradation of its accuracy at distances 100 to 150 km beyond the triad base-line.

5.2 Surface Winds

Surface winds are required inputs to models relating the environment to IR missile sensor performance. The main effect is to reduce thermal contrast by increasing thermal conduction between target/background surfaces and the atmosphere. The greatest effect will occur during the day when the differential absorptive rates of these surfaces are most pronounced. Winds are useful for providing realtime information and for predictive purposes. In addition, in lieu of a ground-implanted visibility sensor, a measurement of winds in conjunction with temperature and relative humidity might provide an important inference of fog presence.

Winds ideally are monitored by an instrument set out on flat, unobstructed terrain at an arbitrary height of 10 m. The distance between any obstruction and the anemometer should be at least 10 times the height of the obstruction above anemometer ground level. In practice, compromises must be made in anemometer location. To correct anemometer readings to standard conditions, Eq. (10) can be used, where r_h and r_{10} are the windspeed at a height of h and 10 m, respectively.[24]

$$r_h = r_{10}\{0.233 + 0.659 \log_{10}(h + 4.75)\} \quad . \tag{10}$$

Using this relationship, Figure 7 shows the departure from standard wind conditions with anemometer height above the surface. Though a measurement obtained from a ground implant can be corrected for non-standard conditions (it is presumed that the sensor will be at a known and fixed height), its ultimate location is

24. (1956) Handbook of Meteorological Measurements, Part I, Her Majesty's Stationery Office, London, p. 201.

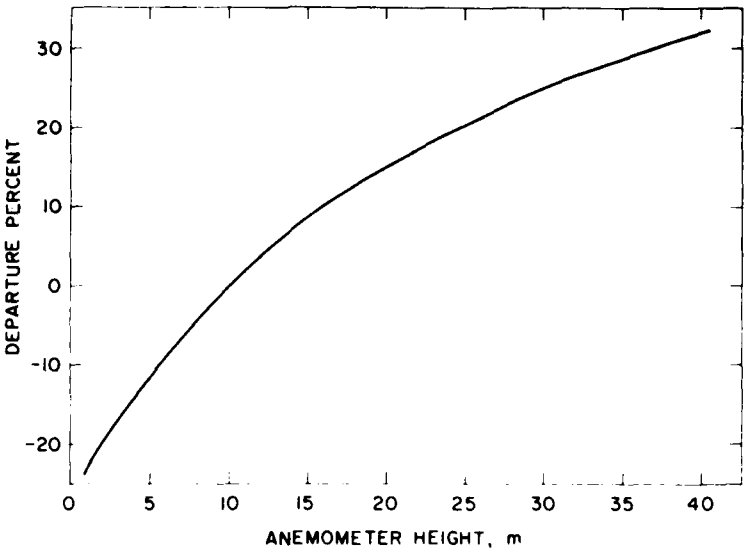

Figure 7. Wind Measurement Departure From Standard Conditions of Anemometer Exposure

almost completely determined by the vagaries of the wind during sensor deployment. If it lands in high grass, brush, forest, water, rough terrain, or hillside, the measurement is virtually useless. The measurement of winds in hollows and valleys, which might provide information on fog presence or its development, is exactly where it would be most suspect. The measurement would be extremely site-dependent and could be significantly different several hundred yards away. Thus, an anemometer positioned on the side of a valley could be indicating winds due to drainage conditions, while winds at its base could be relatively calm. Though these might represent worst case situations, it does raise the general issue of the "representativeness" of point observations. It should be recognized that, even under ideal conditions, site representativeness often can only be determined after a statistical analysis of field-site observations.[25]

An important consideration in the measurement of wind parameters is the selection of sensor time constant, sampling rate, and data-averaging period. In a benign environment one normally has the luxury of using a sufficiently long averaging period and a correspondingly appropriate sampling rate for optimum

25. Nappo, C.J., et al (1982) Meeting review of the workshop on the representativeness of meteorological observations, June 1981, Boulder, Colo., Bull. Am. Meteorol. Soc. 63:761-764.

monitoring. In general, the error in estimates of wind parameters decrease with the increasing length of the observational period. Equation (11) shows the relation between the requisite averaging period and measurement accuracy, where T is the averaging period, "ε" is the desired accuracy, $\bar{f}$ and $\bar{f'}^2$ are ensemble mean and variance, respectively, for a random process f of integral time scale τ,[26]

$$T \cong \frac{2\tau(\bar{f'})^2}{\bar{f}^2 \varepsilon^2} \quad . \tag{11}$$

Table 7 from Haugen[24] shows typical error estimates for various random processes for time-averaging periods of 15 and 60 min based upon this equation.[27] In these calculations an integral time scale of 1 sec was assumed for all processes.

Table 7. Percentage Error of Estimates for Selected Random Processes and Averaging Periods, T

Process	T = 15 min	T = 60 min
Mean windspeed	1%	0.5%
Windspeed variance	7%	3.5%
Heat flux	10%	5.0%
Reynolds Stress	20 to 100%	10 to 50%

It is evident that, if one is merely interested in local mean windspeed estimates with accuracies no better than 10 to 20 percent, a time-averaging period of only a few seconds will suffice. If, however, these estimates are also to be representative of a broad surrounding area (say 1 km in diameter), then the averaging period must be considerably increased to include all scales of turbulence and to minimize spatial inhomogeneities. For representative coverage a 15-min averaging period would be more appropriate.

The selection of sensor sampling rate and time constant will depend upon desired wind parameters of interest. If windspeed variance or higher moments

---

26. Lumley, J. L., and Panofsky, H. A. (1964) The Structure of Atmosphere Turbulence, Interscience Publishers, N. Y., p. 27.

27. Haugen, D. A. (1978) Effects of sampling rates and averaging periods in meteorological measurements, 4th Symposium on Meteorological Observations and Instrumentation, Denver, Colo., April.

are desired, higher sampling frequencies are indicated. Again, if only mean windspeed is required then a sensor with relatively long time-constant (say 5 min) could be used such that after about 15 min it has essentially reached steady-state with the environment. An RPV returning to the implant area after this elapsed period would then have to acquire, in principle, only one sample transmission to get an estimate of the 5-min windspeed. Assuming the operational scenarios can be altered so that the ground implant is deployed early in the RPV ingress of the target area, a longer time constant can be accepted resulting in a longer effective averaging period.

5.2.1 HOT WIRE ANEMOMETERS

No attempt will be made to review the extensive variety of measurement techniques available for the monitoring of surface winds. Most of these are unsuitable for use in a tactical ground-implant. Many use inherently fragile components, for example, cups/propellers; many are prohibitively expensive, for example, sonic and laser anemometers; others are not sensors of choice because of reasons of size, weight, or power.

A particularly attractive candidate, having most of the desired characteristics is the hot wire anemometer. Some versions of this instrument are sufficiently rugged to withstand dropsonde deployment, have a more than adequate speed of response (in fact, better than BWOFS requires), and have acceptable physical characteristics. It is anticipated that, any wind sensor selected will require repackaging and design of a suitable electronics package to conform to our specific operational requirements. Two probes manufactured by TSI Inc., St. Paul, Minn., warrant consideration in a BWOFS ground-implant, namely, Velocity Transducer Models 1610 and 1620. Features of these probes taken from company product literature are given in Tables 8 and 9.

Table 8. TSI Model 1610 Velocity Transducer

Input power:	+9 Vdc 250 ma max
Output impedance:	less than 100 ohms
Repeatability:	±0.1% reading ±0.05% F.S.
Response time:	0.1 sec
Environmental temperature range:	0 to 70°C
Output voltage:	approx 1 to 5 Vdc non-linear
Accuracy:	±1.5% reading ±F.S. over 50:1 range
Velocity range:	0 to 3 m/s and 0 to 30 m/s
Temperature compensation:	0 to 40°C. Other ranges on request.

Table 9. TSI Model 1620 Omnidirectional Air Velocity Transducer

Input power:	+9 Vdc 250 ma max
Output impedance:	less than 100 ohms
Repeatability:	±0.2% reading ±0.1% F.S.
Response time:	2 sec
Environmental temperature range:	0 to 70°C
Output voltage:	approx 1 to 5 Vdc non-linear
Accuracy (typical):	±10% reading over 0.2 to 3 m/s (over a 240° solid angle)
Velocity range:	0 to 3 m/s
Fluid temperature range:	-50 to 100°C
Temperature compensation:	0 to 40°C

General physical dimensions of the model 1610 are shown in Figure 8. The probe is a rugged and metal-clad sensor and should be able to withstand high G loads. Probe lengths in both the 1610 and 1620 models come in non-standard sizes. The manufacturer claims that the probe can be up to 15° off-vertical before introduction of significant measurement error.

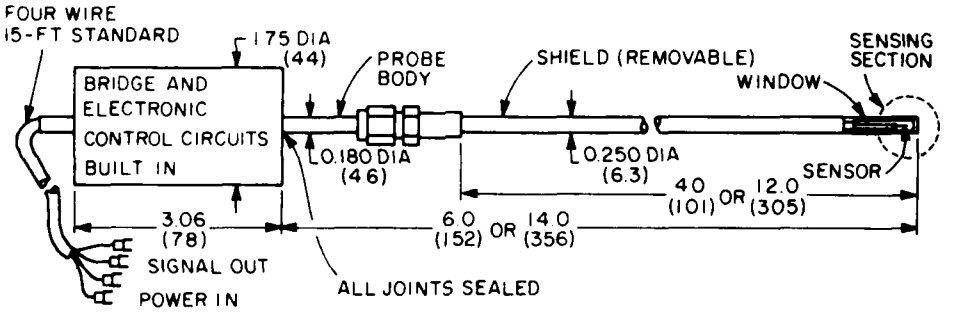

Figure 8. TSI Model 1610 Velocity Transducer

Though the model 1620 is primarily used for very low windspeeds (less than 3 m/s) it has sensitivity up to 10 m/s. A solid, spherical metal tip provides for insensitivity to wind direction over a broad solid angle; for use as an implant, the sensor could be up to 30° from the vertical before this introduction of significant measurement error. Though the sensor tip is not as rugged as in the model 1610,

as long as it is not physically struck, it should be able to survive anticipated ground-impact velocities.

Though a certain modest amount of flexibility exists in TSI sensor orientation to the wind flow (up to 30° off-vertical) the design of an implant to ensure deployment within these tolerances will provide a strong challenge.

6. OPTICAL AND IR TRANSMISSION

6.1 Background

Optical and IR transmission information are two of the requirements identified as being critical to TAF operations. A knowledge of E-O transmission properties in the target area are necessary inputs to the "fragging" (weapons uploading) process and, importantly, provide the fighter pilot with invaluable information on expected visibility conditions. The requirement for both visibility and "seeability" measurement accuracies (Table 1) are ±20 percent over the range of 0.1 to 10 km. Current efforts in the IR are directed toward characterization of atmospheric transmission in the 8 to 12 μ region. As weapons systems utilizing other wavelengths become available, additional operational requirements are anticipated. Though it may be technically feasible to design E-O instrumentation for deployment by dropsonde, as well as by RPV; cost constraints for expendable devices would, with the possible exception of a visibility meter, preclude their use. Therefore, initial technical development of sensors has been directed toward non-expendable, RPV-delivered instrumentation.

The derivation of visibility or visual range is usually accomplished with instruments that directly measure the contrast between object and background or by the measurement of the extinction coefficient with its translation into visual range. Telephotometers are examples of the first type; these require accurate sighting and are not amenable to automation for tactical deployment. The second type, involving the measurement of attenuation, is most commonly performed with transmissometers and light-scatter meters. Transmissometers measure light transmission over a known or fixed path which, with an assumption about the optical contrast threshold value, is converted into meteorological range. To obtain requisite sensitivity, pathlengths are usually on the order of hundreds of feet. The development of a short-path transmissometer suitable for the BWOFS is not an attractive solution. The use of scatter-meters (nephelometers) for estimating visibility is widespread and is a mature technology. Its use in estimating visibility is based upon the fact that, in the absence of clouds, fog, or precipitation, visibility is predominately influenced by light scattered by atmospheric aerosols; scattering at the molecular level and absorption are higher-order

effects. Thus, a measurement of the aerosol scattering coefficient could serve to establish total extinction and, hence, visibility. The development of such a device suitable for this program was initiated with HSS Inc., Bedford, Mass.

The estimation of infrared extinction using nephelometry is not so straightforward, particularly in the 8 to 12 μ region. Sensor design is much more demanding than in the optical region and, in addition, the scattering coefficient cannot be directly equated to total extinction since absorption processes cannot be neglected. Rather than assuming the more difficult task of developing an instrument operating directly in the region of interest (that is, 8 to 12 μ) a decision was made to develop a duel-wavelength nephelometer with the expectation that its output can, ultimately, be used to infer the variable of interest. This development, also with HSS Inc., is described in this section.

6.2 The HSS Visibility Meter

In this section, the overall design and characteristics of the nephelometer built for this program by HSS Inc., Bedford, Mass., will be described. Much of this will also be pertinent to Section 7.2, which is titled In-Situ Detection.

The HSS nephelometer is a fixed-angle forward-scatter device. A schematic diagram of the optical system is shown in Figure 9 and pertinent characteristics are provided in Table 10. The reason for the selection of 0.88 μ is the availability of small, inexpensive, low-power, light-emitting diodes. These are easily modulated electronically and obviate the need for mechanical chopping. A laboratory model was tested at the Calspan Corporation's Environmental Fog Chamber over a wide range of fogs and hazes. Conditions included large and small droplet fogs, and hazes at both high and low relative humidities to ensure as wide a spectrum of aerosol size distributions as possible. Though the required equivalent visual range for the sensor is 0.1 to 10 km, the test conditions were extended to determine the maximum operational sensitivity of the instrument. To this end, external to the sensor, a signal conditioner with a gain of 25 was employed for resolution of the smaller attenuation coefficients. Figure 10 is a graph of the test results. Of major significance is the fact that, within operational requirements for accuracy, a universal calibration equation can be used that will cover most anticipated, environmental scattering phenomena.

The prototype nephelometer is shown in Figure 11. Though considerable effort was made to keep its physical dimensions to a minimum, there is still room for further weight reduction. The instrument contains considerable heavy-gage metal which could, in a final model, be reduced or replaced by plastic construction. A 1-lb weight reduction is a conservative projection.

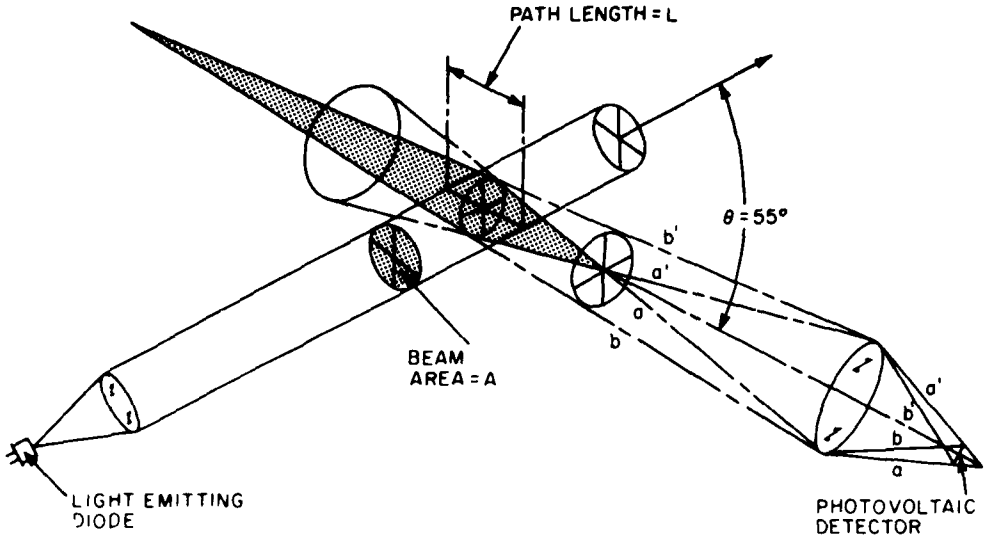

Figure 9. Schematic Diagram of the HSS Nephelometer Optical System

Table 10. Airborne Nephelometer Characteristics

Scattering Volume:	
X-sectional area:	1 cm^2
Pathlength:	1 cm
Scattering angle:	55 ± 6°
Transmitter:	
IRED source power:	12 mw
Center wavelength:	8800 mA°
Optical bandwidth:	800A°
Receiver:	
Detector:	Silicon photovoltaic
Useful detector area:	5.1 mm^2
Electrical bandwidth:	0.5 Hz
Time constant:	0.5 sec
Sample rate:	0.5 sec
Power Input:	10 w at 28 Vdc
Power Output:	0 to 10 Vdc
Weight:	~ 5-1/2 lb
Size:	3-1/2 × 4-1/2 × 14-1/2 in.

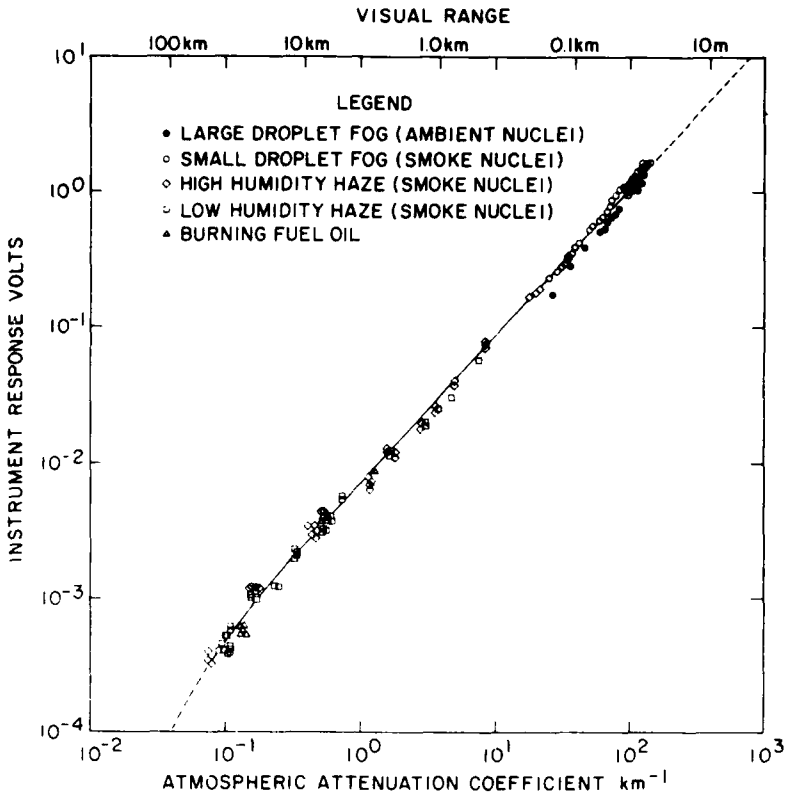

Figure 10. HSS Nephelometer Test Results

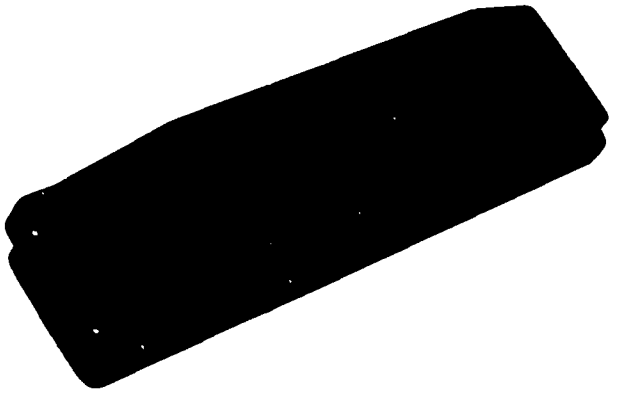

Figure 11. The HSS Visibility Meter

If, in addition to visual range, the nephelometer is to provide an indication of cloud presence (Section 7.2.1), conflicting requirements for time constants have to be resolved. Resolution of cloud boundaries require a short time constant, while longer sampling times will improve the accuracy of extinction measurements through an improvement in signal-to-noise. Another factor to be taken into account is the flight profile to be employed. During horizontal monitoring of extinction, one could assume conditions of horizontal homogeneity and, thus, not be too concerned with the rate-of-change of this variable, whereas, in vertical profiling, this assumption is not necessarily valid. Since the utilization of the nephelometer to characterize cloud-field properties presupposes a vertical profiling scenario (Section 7.4), time constants appropriate to this mode will be examined.

In all deployment scenarios of the nephelometer via RPV, it will be assumed that the speed of the vehicle is more than adequate to ensure that a representative atmospheric volume has been sampled. If the shortest time constant anticipated is 0.1 sec and the slowest vehicle speed is 50 mph, the integrated sample volume monitored by the nephelometer will be about 0.2 l; this volume will provide for adequate sampling statistics.[28]

Both the laboratory and the prototype visibility meters were field-tested at AFGL's Weather Test Facility at Otis Air Force Base. Intercomparisons with standard transmissometers and with forward-scatter meters have served to establish relative accuracies as functions of visual range and instrumental time constraints. Tables 11 and 12 give the coefficients of dispersion (that is, standard deviations divided by means) for the prototype sensor at an approximate visibilities of 10 km and 100 m, respectively. It can be seen that the largest errors are associated with daytime measurements at the maximum range requirements of 10 km. Thus, for example, the daytime error should range between 11 and 85 percent, depending upon the time constant selected. The time constant used will, of course, impact upon the spatial resolution. Table 11 implies that all accuracy requirements can be met with a $\lambda = 2$ sec if the light source flux can be increased by a factor of three. The coefficients of dispersion for $\lambda = 2$ will be correspondingly reduced by a third, such that the estimated accuracies are within ±20 percent. Most, if not all of this increase in light flux can readily be obtained by operating the LED at a higher current level. Major increases in light flux can also be obtained by decreasing the central scatter angle of the nephelometer from 55 to about 45°; however, this would necessitate a redesign of the instrument. The analysis that follows assumes that in an engineered instrument this factor of 3 increase in flux can be achieved.

---

28. Hansen, D. F. (1982) Development of an Airborne Visibility Meter, AFGL-TR-82-0328, AD A124276.

Table 11. Relative Instrumental Error of the AVM for Various Time Constants of Integration at a Visual Range of 10 km

Time Constant (sec)	Coefficient of Dispersion	
	Daytime	Nighttime
$\lambda = 60$	±0.110	±0.049
$\lambda = 15$	±0.22	±0.098
$\lambda = 5$	±0.38	±0.170
$\lambda = 3$	±0.49	±0.219
$\lambda = 2$	±0.60	±0.27
$\lambda = 1$	±0.85	±0.380

Table 12. Relative Instrumental Error of the AVM for Various Time Constants of Integration at a Visual Range of 100 m

Time Constant (sec)	Coefficient of Dispersion	
	Daytime	Nighttime
$\lambda = 60$	±0.011	±0.0049
$\lambda = 15$	±0.022	±0.0098
$\lambda = 5$	±0.038	±0.017
$\lambda = 3$	±0.049	±0.022
$\lambda = 2$	±0.060	±0.027
$\lambda = 1$	±0.085	±0.038
$\lambda = 0.5$	+0.120	+0.054

To assess the adequacy of an approximately 2-sec time constant for extinction measurements, the deployment scenario and expected extinction coefficient rates-of-change must be examined. Extensive aircraft measurements, both in the U.S. and in Europe, by Duntley et al,[29] indicate that non-cloud aerosols are usually homogeneously distributed in a well-mixed boundary layer that exists to about 1500 ± 1000 m, and in which the extinction coefficient is, essentially, constant.[29, 30] These observations were the basis for Huschke's construction of the Weather Effects on Tactical Target Acquisition (WETTA) model.[31]

In this model Huschke also assumed an abrupt discontinuity at the top of the mixing layer having a constant value of visibility of 83 km ($\sigma = 0.05\ km^{-1}$). A variation of this model would consider an exponentially-decreasing extinction coefficient from the top of the boundary layer and extending upward. Other models, such as Elterman's,[32] postulate an exponentially-decreasing extinction coefficient from the surface to the top of the atmosphere.[32]

It should be apparent that, nephelometer operation within a well-mixed boundary layer, having slowly-varying or nearly-constant optical properties, will pose no special monitoring problems. For an exponentially-varying vertical profile a detailed analysis will be required. If we assume that the nephelometer is being deployed at a constant rise/descent rate, the extinction coefficient would be seen to vary with time according to

$$\sigma_e = \sigma_0 \exp(-\beta t) \quad , \tag{12}$$

where σ_e is the initial extinction, σ_e is the expected environmental value at time t, and β is a coefficient dependent upon extinction rate-of-change. Using typical values for extinction at the surface and 10,000 ft, namely, $0.83\ km^{-1}$ and $0.065\ km^{-1}$, respectively, and an ascension rate of 5000 ft min^{-1}, we calculate a $\beta = 0.0212\ sec^{-1}$. It can also be shown that the appropriate relation describing expected sensor response is given by,

---

29. Duntley, S.Q., Johnson, R.W., and Gordon, J.I. (1972) Airborne Measurements of Optical Atmospheric Properties in Southern Germany, Visibility Laboratory, UCSD, San Diego; AFCRL-72-0255, AD 747490.

30. Duntley, S.Q., Johnson, R.W., and Gordon, J.I. (1972) Airborne and Ground-Based Measurements of Optical Atmospheric Properties in Central New Mexico, Visibility Laboratory, UCSD, San Diego; AFCRL-72-0461, AD 751936.

31. Huschke, R.E. (1976) Atmospheric Visual and Infrared Transmission Deduced From Surface Weather Observations: Weather and Warplanes VI, The Rand Corporation, R-2016-R.

32. Elterman, L. (1968) UV, Visible, and IR Attenuation for Altitudes to 50 km, AFCRL-68-0153, AD 671933.

$$\frac{\sigma_e}{\sigma_i} = \frac{[(\beta\lambda - 1)\exp(t/\lambda)]}{\beta\lambda \exp(\beta t) - \exp(t/\lambda)} \tag{13}$$

where σ_e and σ_i are environmental and sensor indicated values, respectively, and λ is the sensor time constant. Figure 12 is a plot of σ_e/σ_i as a function of sensor time constant. For a time constant of 2 sec, the maximum deviation in the measurement at steady-state will be approximately 5 percent; this will not appreciably alter the anticipated accuracy that will have an overall rms error of 20.6 percent. Thus, due to the relatively slow variation in extinction with height for an exponential environment, the nephelometer should be able to provide measurements within the design accuracy. However, it should be appreciated that the atmospheric models alluded to above are highly idealized. While the distribution of aerosols may be relatively constant in the boundary layer, or relatively exponential with altitude, additional structure should always be expected. Changes of 2 or 3 in the scattering coefficient, over a scale of a few hundred meters, should not be considered unusual. Aerosol structure of such a nature could impose more serious demands upon the selection of nephelometer time constant(s). Also impacting strongly upon time constant selection, or the anticipated degradation of measurement accuracy, is the ultimate operational scenario selected. Relaxation of RPV rate of rise/descent requirements could materially enhance sensor capability. If we consider an RPV ascending/decending at a rate of 5000 ft min^{-1}, three time constants (that is, 6 sec) will provide for spatial resolution of the scattering coefficient over, approximately, 500 ft in the vertical. The sensor's operation at low altitudes and in highly-polluted urban atmospheres, or in target areas in which battlefield contaminants are present, will also pose special problems that will have to be specifically addressed.

6.3 Short-Wave IR Nephelometer (SWIRN)

A brief description will be given of the contractual effort with HSS Inc., for the development of a SWIRN. A prototype instrument was constructed that has undergone limited chamber testing. A field-test program for its continued evaluation was initiated. However, during the period of test, no restrictions to visibility occurred.

The SWIRN is a dual-wavelength nephelometer operating at 0.55 and 2.25 μm. The selection of 0.55 μm rather than the 0.89-μm region used in the visibility meter is partly due to the desire to maximize the separation between wavelengths, in hope that it will facilitate extrapolation of the scattering coefficient to the 8 to 12 μm region. Also, this would provide us with an alternative wavelength

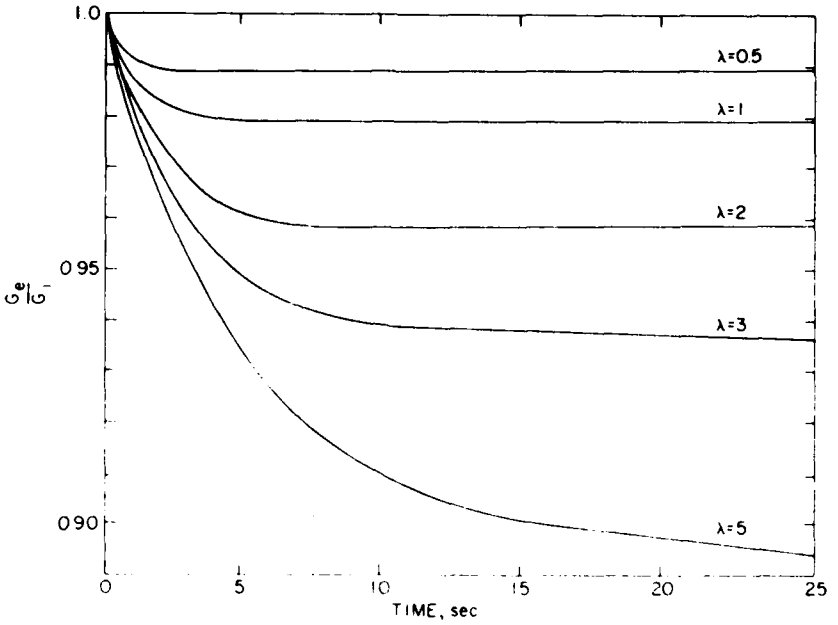

Figure 12. Nephelometer Response to an Exponential Change of Extinction

that could be utilized if a distinct advantage for its use became apparent. One advantage of 0.55 μm is that it is the region in which visual range is defined. Another is the fact that a single source (that is, a tungsten lamp), with suitable filtering, can be used for both wavelength regions. General SWIRN characteristics are provided in Table 13.

The SWIRN was tested in the Calspan Corporation's Environmental Fog Chamber, and RH test involved nine fog and five haze conditions. Visible wavelength extinction was measured with three instruments, an MRI Integrating Nephelometer 1550B ($0.01\ km^{-1} < \sigma < 10\ km^{-1}$) and two Calspan-built transmissometers operating over pathlengths of 18.3 and 2.7 m. Stated accuracies in the scattering coefficient for the nephelometer are $\pm 0.1\ km^{-1}$ from 0 to $1\ km^{-1}$ and $\pm 1\ km^{-1}$ from 1 to $10\ km^{-1}$. For the transmissometers, the extinction coefficient was computed from Bouguer's Law ($I = I_o\ e^{-\sigma x}$). Estimated accuracies are ±10 percent or $\pm 0.5\ km^{-1}$ (whichever is greater) for the 18.3 m pathlength transmissometer and ±10 percent or $\pm 4\ km^{-1}$ (whichever is greater) for the 2.7-m pathlength transmissometer.

Table 13. SWIRN Specifications

Optical characteristics, channel 1 (visible):	
Central wavelength:	0.55 μm
Optical bandwidth:	0.08 μm
Detector:	Silicon photovoltaic
Optical characteristics, channel 2 (IR):	
Central wavelength:	2.25 μm
Optical bandwidth:	0.5 μm
Detector, peltier-cooled:	PbS
Window:	Sapphire
Heater power:	4.5 W
Source characteristics:	
Type:	Tungsten lamp
Power:	20 W
Chopper frequency:	533 sec^{-1}
Scattering angle coverage:	
Central angle:	55^{o}
Angular spread:	$\pm 5^{o}$
Sample volume:	4 cm^{3}
Output characteristics (both channels):	
Voltage:	Analog
Range:	0-10 V
Time constant (basic instrument):	0.5 sec
Time constant with signal conditioner:	15 sec
Power Requirements:	50 W
Physical characteristics:	
Weight (excluding power supplies):	9.5 lb
Size:	17.5 in. L × 4 in. W × 5.5 in. H

The IR wavelengths monitored were 2.117 to 2.325 μm and 9.13 to 10.33 μm, using the 18.3-m path, a 900^{o}C blackbody source, and a HgCdTe, liquid nitrogen-cooled detector. Estimated accuracies prior to chamber filtrations, pressurization or expansion, are ±10 percent or ±1 km^{-1}, whichever is greater. During or after those operations, the accuracy is estimated to be ±10 percent or ±3 km^{-1}, whichever is greater.

Other information that was available during the runs included aerosol concentration and size distribution, as well as fog droplet size spectra.

Figures 13 and 14 show calibrations of the visible channel for fog and haze episodes, respectively. As with the HSS visibility meter (Section 1.6.2) operating at 0.89 μm, considering the uncertainties in the Calspan sensors, we are reasonably confident that a single calibration curve can be used for most restrictions to visibility. Not shown in the figures are the runs in which high concentrations of white phosphorus or KCl/NaCl mixtures were used; the resultant aerosols are not considered typical of naturally-occurring substances, or, as in the case of the salts, not found in such high concentrations.

Figures 15 and 16 are calibrations for the SWIRN IR channel. The calibration curve for fogs are reasonably distributed over the various runs. Different runs for haze conditions appear to have different scattering properties. It has been observed that the aerosol size distributions in these hazes are skewed to sizes smaller than normally found in the free atmosphere and do not have the "tail" of the large particles usually expected. Lacking adequate field-testing of the SWIRN, it is felt that the full capability of the IR channel has not been established. Based upon chamber testing, SWIRN performance characteristics for the present instrument are given in Table 14. Taking into account the experience gained in the design of the prototype visibility meter, it is anticipated that improvements can be incorporated into a second-generation SWIRN having the capabilities enumerated in Table 15.

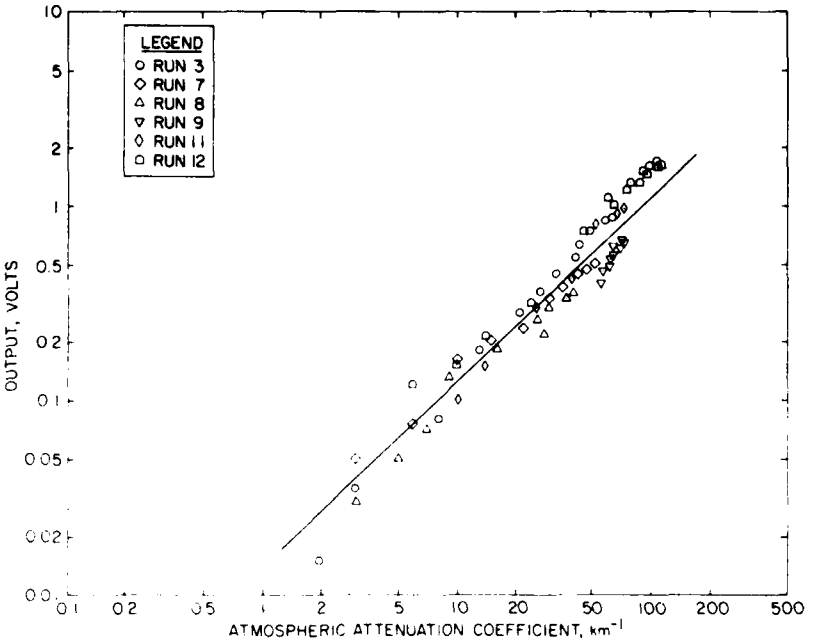

Figure 13. SWIRN Calibrations in Fog (Visible Channel)

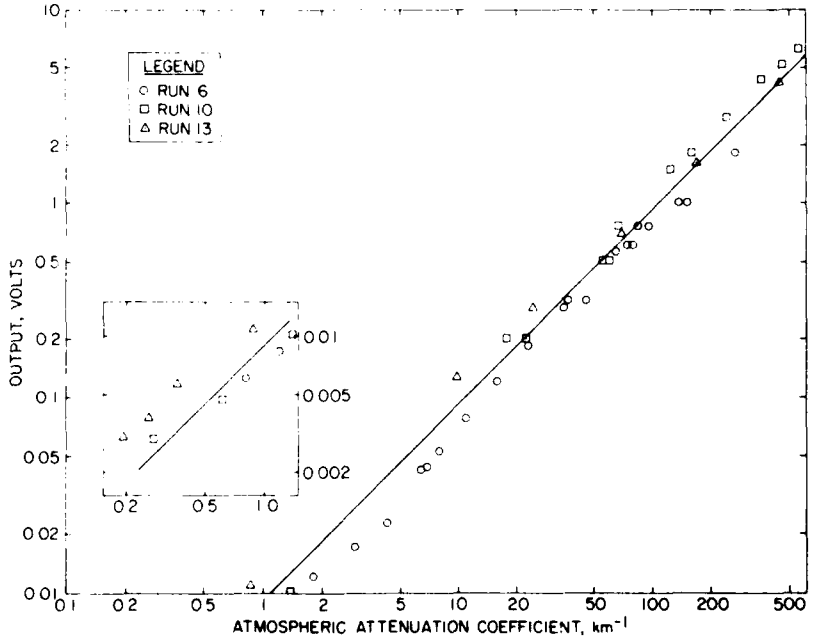

Figure 14. SWIRN Calibrations in Haze (Visible Channel)

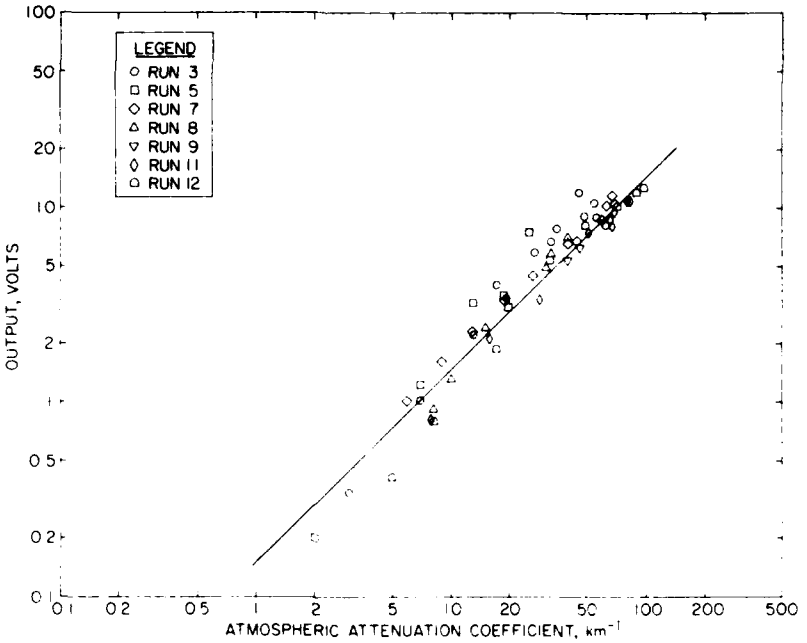

Figure 15. SWIRN Calibrations if Fog (IR Channel)

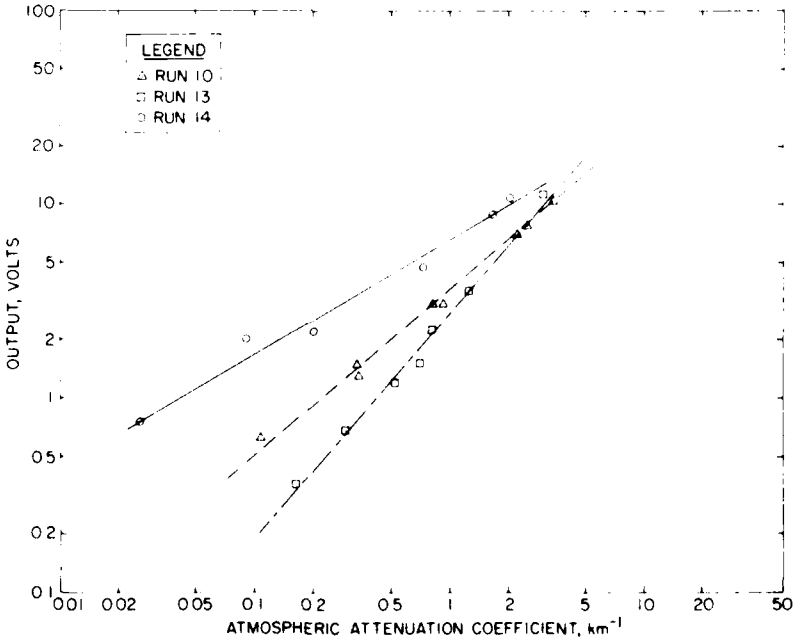

Figure 16. SWIRN Calibrations in Haze (IR Channel)

Table 14. Current SWIRN Capability Determined From Calspan Tests; Based on 15-sec Time Constant

Channel 1 (visible):		
Scattering coefficient range:		1000 to 0.1 km^{-1}
Visual range:		3 m to 30 km
Accuracy (based on 15-sec time constant):		
Relative error:	at 30 km	100%
	at 10 km	20%
	3 m to 5 km	<15%
Channel 2 (IR):		
Scattering coefficient range (at 2.25 μm):		
Fog:		70 to 1.5 km^{-1}
Haze:		1.5 to 0.006 km^{-1}
Seeability range (estimated for 8 to 12 μm):*		
Haze:		1.5 to 384 km
Accuracy:		
Relative error:	at 150 km	100%
	at 40 km	20%
	40 m to 25 km	15%

*Seeability is that range at which a sensor can see, acquire, or lock-on to a target. It has been assumed here that the total extinction at 8 to 12 μm is comparable to the observed scattering coefficient at 2.25 μm and that a value of 0.05 is used for T_{thr}, the threshold transmission value.

Table 15. Projected SWIRN Capability: For 2-sec Time Constant

Channel 1 (visible):		
Scattering coefficient range:		100 to 0.3 km^{-1}
Visual range:		30 m to 10 km
Accuracy (based on 2-sec time constant):		
Relative error:	at 10 km	100%
	at 2 km	20%
	30 m to 115 km	15%
Channel 2 (IR):		
Scattering coefficient range (at 2.25 μm):		100 to 0.016 km^{-1}
Seeability range (estimated for 8 to 12 μm):		20 m to 575 km
Accuracy:		
Relative error:	at 575 km	100%
	at 100 km	20%
	20 m to 75 km	15%

7. CLOUD FIELD CHARACTERIZATION

7.1 Background

The characterization of clouds in the target area is of vital concern to mission planners and the tactical fighter pilot. Typical operational scenarios in support of PGMs call for a low ingress to the target area at an elevation of a few hundred feet (AGL) with a "pop-up" to 500 to 1000 ft when approaching the anticipated acquisition range. Depending upon the particular weapon system, the pilot executes a "launch and leave" maneuver immediately before or after target "lock-on". Modification of the optimum aircraft flight pattern, due to adverse cloud conditions, greatly increases the physical threat, leading to higher aircraft attrition rates. Knowledge of conditions in the target area will not only increase the effectiveness of the mission, but will also reduce the number of diverted sorties and missed opportunities. The value of this information cannot be overemphasized, it is the single-most important weather requirement for PGM support. The specific cloud requirements were identified in Table 1.

For the BWOFS program, two distinct approaches have been given consideration; one is a remote radiometric technique and the other is an in-situ nephelometric method. Both methods will require flight test and evaluation, though a nephelometer embodying the requisite characteristics for a tactical weather sensor has already been fabricated and tested in an environmental chamber and, to a limited extent, in the field.

The technique ultimately to be employed will be heavily influenced by the operational scenarios, dictated by considerations of physical survivability and, navigation communication, etc., chosen for the delivery vehicle. If a high-altitude overflight of the target zone is used, either a remote sensor aboard the RPV or multiple dropsondes containing suitable in-situ sensors would be required. Complete characterization of a multilayered cloud deck with the radiometric method could require passes at more than one altitude, increasing its vulnerability to a greater variety of enemy ordnance. The in-situ method provides for greater vertical definition of the cloud field, but is also subject to increased vulnerability at low altitudes. Engineering studies and life-cycle cost analysis to be performed in FY83 will provide the user commands with the basis for making a selection among operational scenarios on the basis of cost and performance, was well as system survivability.

7.2 In-Situ Detection

7.2.1 THE HSS NEPHELOMETER

One method for the detection of cloud presence is the utilization of the HSS nephelometer described in Section 6.2. Nephelometers monitor light scattered by particles suspended in a medium, in this case, water droplets in air. The relatively large signals one would obtain in clouds, as contrasted from non-cloud aerosols, should provide for their unambiguous identification, except for the most extreme combinations of thin clouds and very dense haze.

Requirements for cloud boundary resolution and visual range accuracy are functions of the instrument's time constant. These two requirements which, in turn, are influenced by the deployment scenario, are not necessarily compatible. If indeed, a compromise time constant cannot be found to satisfy both cloud and visual range requirements, it may still be possible to alter the electronic circuitry such that two separate outputs, each tailored to the specific requirement, are available.

For cloud detection, assume that cloud boundaries are to be spatially resolved to within 10 m. Note that this is a program imposed restriction; the operational requirement (Table 1) is ±100 ft. Let us also assume an operational scenario in which the instrument is monitoring a vertical profile at a maximum rate of climb/descent of 10,000 ft min^{-1}. This should be a worst case, considering the currently-available RPV options, but will serve to scope an ultimate performance requirement. A scenario, however, requiring horizontal monitoring would, because of greater possible velocities, be still more demanding. A time constant of about 0.1 sec will resolve cloud boundaries within the prescribed 10 m, and allow for measurement of non-cloud extinction to within 95 percent (that is, 3λ) of the true value. Though the requirement for cloud detection does not call for the measurement of extinction within the cloud, assumptions will have to be made about cloud characteristics. Extinction coefficients in clouds span a broad range from about 2 km^{-1} for thin tenuous clouds to as high as 40 to 50 km^{-1} for extremely dark clouds. Since extinction coefficients in haze seldom are as large as 2 km^{-1}, we will assume that values smaller than this are non-cloud measurements, hence define its boundaries.

To improve the nephelometer response to cloud presence, the full-scale output of 5 V was adjusted to correspond to an extinction coefficient equivalent to approximately 20 km^{-1}. Since the instrument is not required to provide an estimate of extinction within clouds, this will allow for a more rapid recovery upon exiting a cloud.

7.3 Remote Detection

7.3.1 BROADBAND PASSIVE RADIOMETRY

As part of the BWOFS program, a study was initiated to assess the feasibility of utilizing broadband solar and broadband IR radiometric techniques for characterization of cloud field parameters.[33] The study included radiometers to be deployed on RPVs and dropsondes in both in-situ and remote observation modes. When operating in-situ it is assumed that observations are being taken during cloud penetration, whereas in the remote mode, penetration has not occurred. These two modes are complementary and can significantly add to the available information on cloud structure. The two ranges are the 0.3 to 1 μm solar and the 7 to 14 μm IR. The utility of these techniques will require a field-test program to establish instrument sensitivities and resolutions of cloud field parameters to be expected in an operational system.

7.3.2 BROADBAND SOLAR RADIOMETRY

Fifteen inexpensive photodiode detectors operating in the 0.3 to 1 μm region would be employed in a "bug-eye" configuration as shown in Figure 17. Detectors would be assembled in three arrays with detectors in each array displaced 30^{o} from one another. One array would look into the nadir plane, and the other two would look 45^{o} from each side of the nadir plane. It is evident that the output from each detector, when operating in the remote mode, would vary as a function of the observed cloud scene. A serial time analysis of detector output from each array would provide data on cloud parameters. Figure 18 shows the type of output that might be expected from an observation of an idealized cloud form. To quote from the Cox report,

"The width of the N_0^{o} pulse corresponds to the width of the cloud element. The times between the leading or falling edges of the pulses for different nadir angles are directly related to the cloud top height relative to the aircraft, i.e. $h = s(T_{1,0^{o}} - T_{1,30^{o}})/\tan 30^{o}$ where s = speed of aircraft. The broadening of the pulses is principally related to the vertical extent of the cloud, i.e. $W_{\theta} = W_{0^{o}} + Z/\tan(\pi/2-\theta)$. The sum of all pulse widths measured by a given detector yields a direct measure of 'effective cloud cover' at the nadir angle of that detector, i.e.

$$q_{\theta} = \sum_{i=1,n} \frac{W_{\theta_i}}{s\Delta t} \quad ."$$

33. Cox, S.K. (1981) Feasibility Analysis of Cloud Field Property Inference From Broadband Radiometry, AFGL-TR-81-0352, AD A113133.

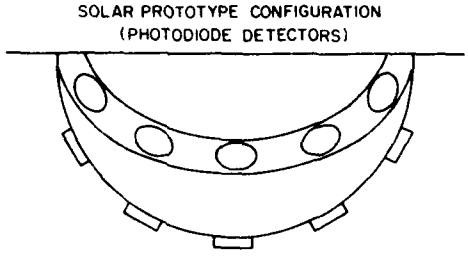

Figure 17. Prototype Solar Detector Array

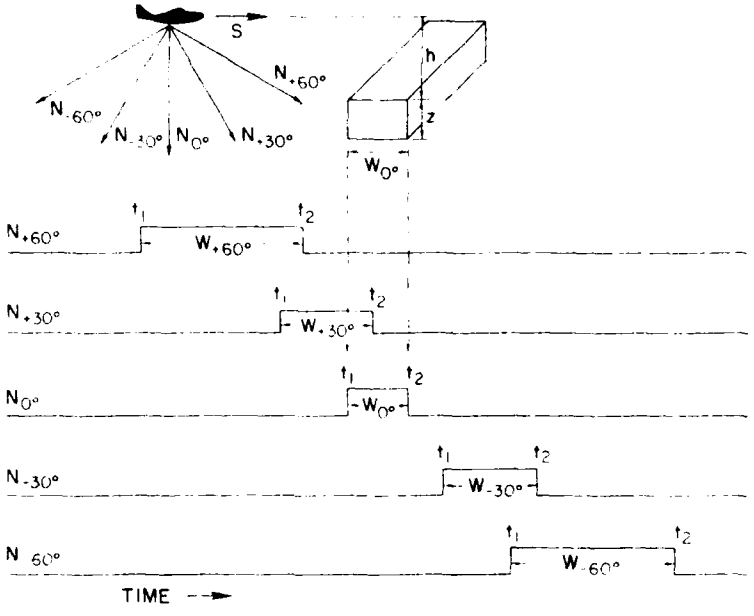

Figure 18. Schematic Representation of Solar Remote Observation Mode

All three detector arrays would provide similar cloud-field parameter information separated by distances proportional to sensor height above the cloud tops. To determine cloud base heights from a remote downward-looking radiometer presumes that a totally overcast sky does not exist. Also, it can be appreciated that multilevel flight observations would greatly enhance the quality of the estimates.

If the radiometer penetrates a cloud, it can be treated as a simple in-situ nephelometer yielding qualitative information of cloud presence. The pronounced divergencies between upward and downward radiances should readily define cloud top boundaries and, to a lesser extent, ceiling. The optical properties within the cloud mass are, also, relatively isotropic compared to the clear air in the upper hemisphere.

The potential exists for solar radiometer deployment from dropsondes. In this configuration, only one upward-looking detector would be used. When passing through a cloud top the received solar component would decrease dramatically and, thus, provide a reliable indication of the cloud boundary. If an upper cloud deck exists, the magnitude of the detector output discontinuity would depend upon upper-cloud deck opacity. Unfortunately, the divergence anticipated at the cloud base is probably not large enough for its identification. The information from a single dropsonde would be very limited and, for maximum effectiveness, would necessitate multiple releases in patterns of the type identified in Section 7.4, Cloud Field Modelling.

7.3.3 BROADBAND INFRARED RADIOMETRY

Radiometric measurements in the 7 to 14 μm region can be made with the sensor configuration shown in Figure 19. As with the solar radiometer, information can be derived from both remote and direct sensing. Radiometers can be deployed such that upper and/or lower hemispheres can be observed (that is, upward and downward observation).

In the remote mode, sensors would provide inputs to the equation shown in Figure 19, where q is fractional cloud amount, L is the output of a wide field-of-view radiometer, N_{CLR}, N_{CLDT} is a narrow field-of-view output representing either an upwelling clear sky radiance or upwelling radiance from a cloud top, and N_{CLDS} is radiance received from the sides of clouds. The remaining unknown in the equation, β, is an assumed cloud aspect ratio, namely, lateral cloud dimension to cloud height.

Cloud top height would be derived from cloud radiance temperature and the equivalent temperature on a temperature-height scale. The temperature-height scale can either be inferred or directly measured. In an RPV deployed radiometer system, ambient temperature and altitude information will be continuously

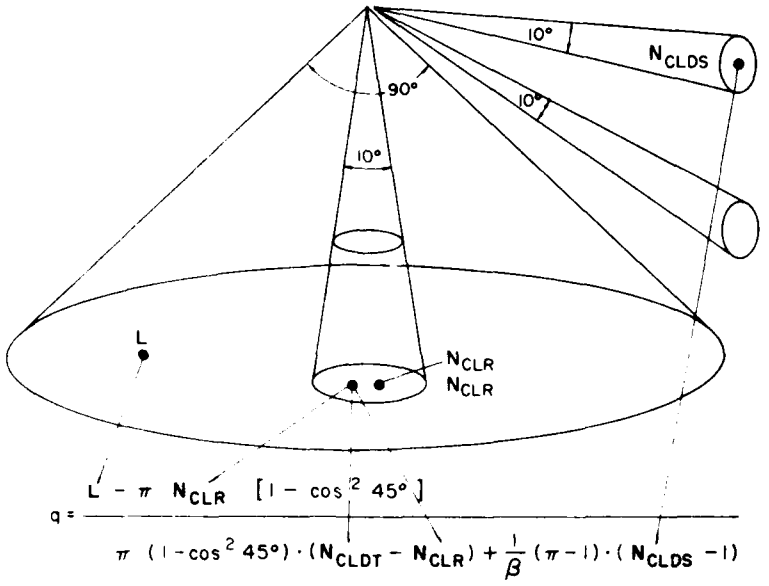

Figure 19. Schematic Diagram of Prototype IR Detector Array

available; operation at two or more altitudes would definitively establish the lapse rate. For RPV operation at a single altitude over the target area, an output of N_{CLR} for ground temperature referencing could also help to establish the lapse rate, to a first approximation.

What has been said about solar observations from dropsondes applies, essentially, to broadband IR measurements. Upward- and downward-looking sensors, however, could provide for an improved IR discrimination of cloud boundaries. It is anticipated that the divergence of upward irradiance will be sufficiently large, such that cloud bases can also be established.

7.3.4 GROUND IMPLANTS

Developing a fixed, groundbased instrument for the characterization of cloud field properties is a major task, even when conditions are ideal for its employment. The development of a remotely-deployed sensor for use in a ground implant and that is also expendable, lightweight, small, rugged, etc., is fraught with great difficulty. The comments that follow apply to any technique, whether passive (for example, radiometric) or active (for example, laser). Let us assume that some inexpensive, non-scanning device could be developed and had the requisite characteristics previously enumerated. How well could it be expected to determine areal cloud cover? For a partial answer to this question, we may refer to an

analysis by Duda, et al, in which the performance of vertically-pointing ceilometers was treated.[34, 35] Using a single instrument with optimum time-averaging of the data, the rmse, $\hat{\sigma}$, in cloud amount estimation was found to be 0.17. Figure 20[35] indicates that if we would like to be correct 80 percent of the time (that is, P_c 0.8), the estimated cloud amount will be within Δ = 0.2 of the correct value for $\hat{\sigma}$ 0.17. With this degree of ambiguity we would justifiably question the merit of using such a system. However, if we increase the number of stations (implants) deployed, the error in the estimate decreases rapidly. If we deploy more than a very few implants, it might be more advantageous to use remote or in-situ airborne instrumentation. Obviously, we are dealing with trade-off issues that are not trivial in nature and require careful consideration.

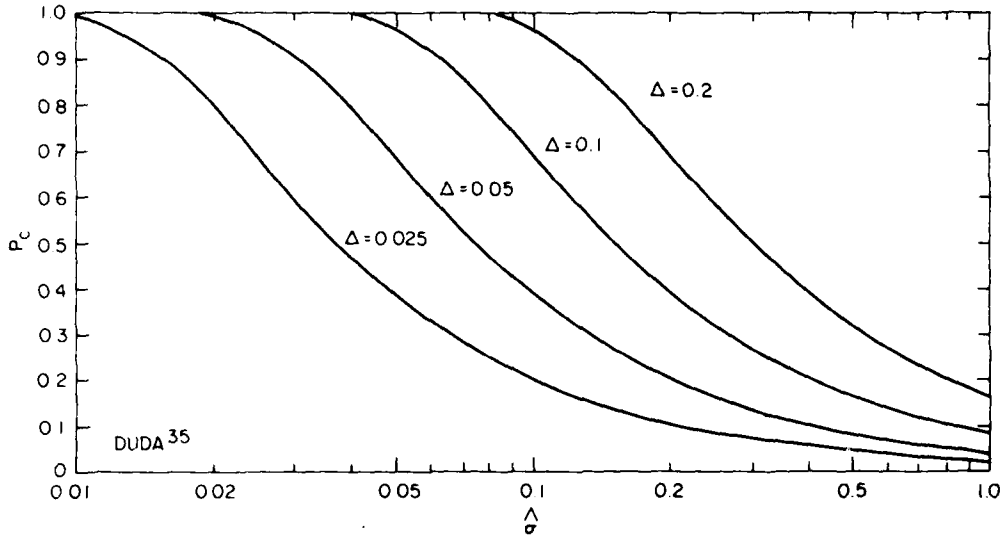

Figure 20. Probability That the Estimated Cloud Amount is Within ±Δ of the True Cloud Amount

34. Duda, R.O., Mancuso, R.L., and Paskert, R.F. (1971) Analysis of Techniques for Describing the State of the Sky Through Automation, Federal Aviation Administration, Report No. FAA-RD-71-52.

35. Duda, R.O., Mancuso, R.L., and Serebreny, S.M. (1973) Automatic instrument system for determining cloud amount, J. Appl. Meteorol. 12:537-542.

A serious objection to the use of implants, at least in a NATO context, is the uncertainty in the type of terrain in which the implant will land. The ceilometer must have an unobstructed view of zenith. If the sensor is in heavy undergrowth or in a wooden area, the measurements are compromised. Admittedly, it is to be expected that the general character of the target zone will be known and this information would enter into any decision as to whether or not a BWOFS should be committed. If a BWOFS were not committed because of terrain considerations, we would be losing part of our flexibility to support operations whenever required. If we deploy implants regardless of anticipated terrain conditions, we risk possible loss of data and/or, what is worse, the acquisition of erroneous data without realizing it.

Because of these considerations, and also because of the problems associated with the acquisition of representative winds (Section 5.2), it is this author's opinion that the desirability of remotely-deployed surface sensors for BWOFS is highly questionable.

7.4 Cloud Field Modelling

The utilization of point measurements (that is, in-situ measurements) of a meteorological variable for the estimation of that variable over a broad two-dimensional area or a three-dimensional space, presumes the availability of a suitable model. During the early development of the HSS nephelometer for cloud presence detection, it was realized that such a model was not available and would have to be *generated*.

A study was initiated to determine the accuracy to which cloud tops, bases, and area coverage could be inferred by an airborne in-situ cloud detector traversing the target space using various selected trajectories.[36] An optimum flight pattern was also to take into account scenario efficiency in terms of time of fuel expenditure. Citing the aforementioned report, three general categories of sampling patterns were examined, "In the first, the target volume is sampled through a succession of horizontal passes that are stepped in altitude, each horizontal sampling consisting of measurements taken along a single pass. The second pattern is identical except that the horizontal sample is now taken along a flight path that is more than a single pass. The third pattern consists of alternate ascents and descents in a tight spiral, the result being that each level is sampled in a pattern of widely separated points." Each sampling pattern was evaluated against an experimental set of data derived from 132 actual cloud fields observed

36. Touart, C.N., Shapiro, R., Mansfield, P.J., and Schechter, R. (1981) Estimating the Tops, Bases, and Amount of Cloudiness From In-Situ Sampling, AFGL-TR-81-0351, AD A113107.

by a Geostationary Operational Environmental Satellite (GOES), as well as theoretical estimates based upon binomial distributions.

Major findings in the study include the following:

a) Horizontal sampling is highly inefficient. Due to the spatial coherence of cloudiness, closely-spaced observations are not statistically independent. The required separation for independence, in the data sets examined, was found to be about 12 km. Thus, the fuel expended and the observations taken between two points separated by this distance are essentially wasted.

b) In horizontal sampling scenarios the vertical profile characterization of cloud fields is directly related to the number of horizontal passes. Altitude resolution of tops and bases for satisfaction of BWOFS requirements would place unacceptable demands upon vehicle endurance and the time needed to fulfill the mission.

c) For both horizontal and vertical sampling patterns, "equal-area" sampling is most efficient. In horizontal sampling, these are passes that divide the plane into equal parts. In vertical sampling each sample point is considered the center of one "equal-area" quadrant into which a given altitude level is subdivided.

d) Vertical sampling is significantly superior to horizontal sampling in terms of fuel economy, and it also has the advantage of providing for greater accuracy in estimation of total cloud amount and of the altitudes of tops and bases.

Differences between horizontal and vertical sampling scenarios may be seen in the following examples where two strategies of each type are analyzed. In Figure 21 the 50 × 50 km grid is traversed horizontally as in H-1 and H-2, or vertically to produce the point patterns in V-1 and V-2 at any given level. For determination of flight time and fuel expenditure, a number of assumptions are made about the flight scenario and vehicle (RPV) performance. The sample volume extends from 1000 to 10,000 ft in the vertical and is sampled at 1000-ft intervals for a total of ten levels for the horizontal strategy. In the vertical strategy, it is assumed that vertical profiles are generated by flying tight spirals of alternate ascent and descent. The RPV was assumed to have the characteristics shown in Table 16. It should not be inferred that a PRESSURS vehicle would necessarily have similar characteristics; it represents a "straw-man" position to highlight the relative differences between the two scenarios.

Table 17 summarizes time and fuel requirements for these sampling strategies, as well as accuracy estimates. P(0.1) percent represents the percentage of the estimates of cloud areal coverage that are within ±0.1 of the correct value. Though the horizontal strategy is slightly more accurate than the vertical strategy (however, providing for only 500-ft resolution of cloud tops and bases) it clearly is inferior, overall, in terms of time and fuel utilization. It must be reiterated that the indicated operational times and fuel expenditures are illustrative, and

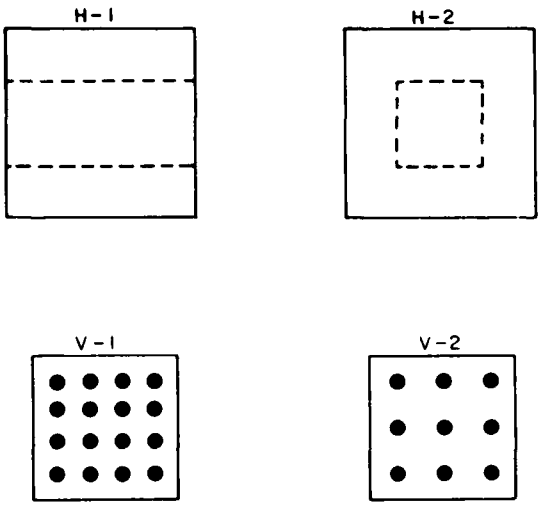

Figure 21. Horizontal and Point (Vertical) Sampling Patterns

Table 16. Typical State-of-the-art Propeller-type RPV Performance

Flight Mode	Airspeed (knots)	Vertical Rate (ft/min)	Fuel Rate (lb/hr)
Horizontal	70	--	8
Ascent	65	500	10
Descent	70	2000	5

Table 17. Time and Fuel Required for Various Sampling Strategies

Pattern Segments	H-1		H-2		V-1		V-2	
	Time (hr)	Fuel (lb)	Time (hr)	Fuel (lb)	Time (hr)	Fuel (lb)	Time (hr)	Fuel (lb)
Horizontal	9.64	77.09	7.71	61.67	1.45	11.56	1.03	8.22
Ascent	---	---	---	---	2.40	24.00	1.20	12.00
Descent	0.08	0.38	0.08	0.38	0.60	3.00	0.38	1.88
Total	9.72	77.47	7.79	62.05	4.45	38.56	2.61	22.10
P(0.1)(%)	96		89		93		81	

represent values for a low-performance vehicle. Analysis of higher-performance vehicles, currently under consideration for BWOFS, will lead to similar conclusions as to accuracy for the various sampling techniques.

In practice, and with the assumption that vertical sampling will be the strategy of choice, the actual pattern employed will be determined by the RPV's operational capability and the acceptable accuracies for estimates of cloud field characterization. Conversion of observations into cloud amounts (total amount and by layers) can be readily accomplished aboard the RPV with simple counting circuitry and microprocessors, thus, obviating the need for transmission of raw data back to the ground terminal.

References

1. (1982) BWOFS Combined Employment Concept (CEC), Air Weather Service.
2. Wexler, A., Ed. (1965) Humidity and Moisture, Volumes I-IV, Reinhold Publishing Corp., N.Y.
3. Wexler, A. (1970) Measurement of humidity in the free atmosphere near the surface of the earth, AMS Monograph II(No. 33):262-282.
4. Brousaides, F.J. (1973) An Assessment of the Carbon Humidity Element in Radiosonde Systems, AFCRL-TR-73-0423, AD 768672.
5. Marchgarber, R.M., and Grote, H.H. (1965) The dynamic behavior of the carbon element, ML-476, Humidity and Moisture, A. Wexler, Ed., Reinhold Publishing Corp., N.Y., pp. 331-345.
6. Morrissey, J.F., and Brousaides, F.J. (1970) Temperature induced errors in the ML-476 humidity data, J. Appl. Meteorol. 9:805-808.
7. Stine, J.L. (1965) Carbon humidity elements—Manufacture, performance and theory, Humidity and Moisture, A. Wexler, Ed., Reinhold Publishing, N.Y., pp. 316-330.
8. (1956) Handbook of Meteorological Instruments, Part I, Her Majesty's Stationery Office, London.
9. (1975) New Thin Film Sensor, Vaisala Ref. No. B235, Vaisala, Inc.
10. Hoehne, W., National Weather Service (1982) Private communication.
11. Nelson, L.D. (1982) Theory, Electro-optical Design, Testing, and Calibration of a Prototype Atmospheric Supersaturation, Humidity, and Temperature Sensor, AFGL-TR-82-0283, AD A121713.
12. (1971) Final Report—NEXAIR Design Analysis, SDO Report 9, NOAA, National Weather Service.
13. (1981) Meteorological Data Error Estimates, Meteorological Group, Range Commanders Council, Document 110-81.
14. Hoehne, W.E. (1980) Precision of National Weather Service Upper Air Measurements, NOAA Tech. Memo. NWS T&ED-16, Sterling, Va.

15. Motchenbacher, C. D. (1977) Mini-Refraction Sonde Laboratory Tests, NADC-76128-30-A.

16. Rosemount Product Data Sheet 2339, Rosemount Inc.

17. Rosemount Product Data Sheet 2064, Rosemount Inc.

18. Cogan, J. L. (1981) Techniques for the Computation of Winds Using RPV Flight Data, White Sands Missile Range, ASL.

19. Rosemount Product Data Sheet 2175, Model 542K Altitude/Airspeed Transducer, Rosemount Inc.

20. Acheson, D. T. (1973) Omega windfinding and GATE, Bull. Am. Meterol. Soc. 55(No. 5):385-404.

21. Govind, P. K. (1973) Dropsonde velocity measurements based on Omega signals, Atmos. Tech. 2:39-42.

22. Morrissey, J. F., and Weiss, B. D. (1975) Dropsonde Wind Measurements Using Omega/Loran Tracking, AFCRL-TR-75-0096, AD A009634.

23. Weiss, B. D., and Morrissey, J. F. (1972) Investigation into Utilization of Loran and Omega Wind Finding System for Measuring Winds Below an Aircraft, AFCRL-72-0399, AD 748275.

24. (1956) Handbook of Meteorological Measurements, Part I, Her Majesty's Stationery Office, London, p. 201.

25. Nappo, C. J., et al (1982) Meeting review of the workshop on the representativeness of meteorological observations, June 1981, Boulder, Colo., Bull. Am. Meteorol. Soc. 63:761-764.

26. Lumley, J. L., and Panofsky, H. A. (1964) The Structure of Atmosphere Turbulence, Interscience Publishers, N. Y., p. 37.

27. Haugen, D. A. (1978) Effects of sampling rates and averaging periods in meteorological measurements, 4th Symposium on Meteorological Observations and Instrumentation, Denver, Colo., April.

28. Hansen, D. F. (1982) Development of an Airborne Visibility Meter, AFGL-TR-82-0328, AD A124276.

29. Duntley, S. Q., Johnson, R. W., and Gordon, J. I. (1972) Airborne Measurements of Optical Atmospheric Properties in Southern Germany, Visibility Laboratory, UCSD, San Diego; AFCRL-72-0255, AD 747490.

30. Duntley, S. Q., Johnson, R. W., and Gordon, J. I. (1972) Airborne and Ground-Based Measurements of Optical Atmospheric Properties in Central New Mexico, Visibility Laboratory, UCSD, San Diego; AFCRL-72-0461, AD 751936.

31. Huschke, R. E. (1976) Atmospheric Visual and Infrared Transmission Deduced From Surface Weather Observations: Weather and Warplanes VI, The Rand Corporation, R-2016-R.

32. Elterman, L. (1968) UV, Visible, and IR Attenuation for Altitudes to 50 km, AFCRL-68-0153, AD 671933.

33. Cox, S. K. (1981) Feasibility Analysis of Cloud Field Property Inference From Broadband Radiometry, AFGL-TR-81-0352, AD A113133.

34. Duda, R. O., Mancuso, R. L., and Paskert, R. F. (1971) Analysis of Techniques for Describing the State of the Sky Through Automation, Federal Aviation Administration, Report No. FAA-RD-71-52.

35. Duda, R. O., Mancuso, R. L., and Serebreny, S. M. (1973) Automatic instrument system for determining cloud amount, J. Appl. Meteorol. 12:537-542.

36. Touart, C. N., Shapiro, R., Mansfield, P.J., and Schechter, R. (1981) Estimating the Tops, Bases, and Amount of Cloudiness From In-Situ Sampling, AFGL-TR-81-0351, AD A113107.

List of Acronyms

AGL	above ground level
APV	Autonomously piloted vehicle
AVM	Airborne visibility meter
BWOFS	Battlefield Weather Observation and Forecast System
CEC	Combined Employment Concept
ECM	Electronic Countermeasures
FEBA	Forward edge of the battle area
GOES	Geostationary Operational Environmental Satellite
GPS	Global Positioning System
IAS	indicated airspeed
INS	Inertial Navigation System
MICNS	Modular Integrated Communication and Navigation System
NEXAIR	Next Generation Upper Air System
NOWCAST	a non-acronym referring to a forecast of present conditions
NWS	National Weather Service
PGM	Precision Guided Munitions
PRESSURS	Pre-Strike Surveillance and Reconnaissance System
RPV	remotely piloted vehicle
SWIRN	Short-Wave IR Nephelometer
TAF	Tactical Air Force
TAS	Target Acquisition System
WETTA	Weather Effects on Tactical Target Acquisition


DAT
ILM